Computer Methods in Applied Mechanics and Engineering 419 (2024) 116683

Contents lists available at ScienceDirect

Comput. Methods Appl. Mech. Engrg.

journal homepage: www.elsevier.com/locate/cma

Reduced Basis modelling of turbulence with well-developed inertial range

Alejandro Bandera Moreno [a], Cristina Caravaca García [b], Tomás Chacón Rebollo [a], Enrique Delgado Ávila [b,*], Macarena Gómez Mármol [b]

[a] IMUS & Departamento de Ecuaciones Diferenciales y Análisis Numérico, Apdo. de correos 1160, Universidad de Sevilla, 41080 Seville, Spain
[b] Departamento de Ecuaciones Diferenciales y Análisis Numérico, Apdo. de correos 1160, Universidad de Sevilla, 41080 Seville, Spain

ARTICLE INFO

Keywords:
Reduced Order Modelling
Large Eddy Simulation
Kolmogorov energy cascade
Reduced Basis method
Greedy Algorithm

ABSTRACT

In this work, we introduce a Reduced Basis model for turbulence at statistical equilibrium. This is based upon an a-posteriori error estimation procedure that measures the distance from a trial solution to the K41 theory energy spectrum. We apply this general idea to build a Reduced Basis Smagorinsky turbulence model through a Greedy Algorithm. We derive some error estimates that make apparent the role of the energy spectrum in the ROM approximation. We carry on some tests for some academic unsteady 2D flows at large Reynolds number, that present well developed inertial spectrum. The methods presents a high efficiency, as the error achieved with the reduced method is 3 to 4 times the ones achieved if the exact error is used in the Greedy Algorithm.

1. Introduction

This paper deals with the building of very fast Eddy Simulation Models for parametric turbulent flows.

Reduced Order Modelling (ROM) nowadays is a methodology in full development to solve parametric Partial Differential Equations (PDEs) with highly reduced computational times. It allows to afford the solution of design, optimization and inverse problems, among others, that were unreachable not long ago (cf. [1–3]).

A very popular ROM basic technique is based upon the Proper Orthogonal Decomposition (POD)(cf. [4,5]). A number of "snapshots" (solutions of the Full Order Method (FOM) for some well-chosen parameter values) is initially computed. The POD allows to determine the dominant patterns of the variety of solutions generated by the snapshots. Combined with some appropriate discretization technique – usually the Galerkin projection of the targeted PDE problem –, allows to construct a low-dimensional surrogate of this problem. A posteriori error estimates allow to estimate the POD-Galerkin ROM–FOM solutions error in terms of the energy carried by the neglected modes. This technique has been extensively applied to the solution of incompressible flows with success (cf. [4,6–10]).

However the POD-Galerkin procedure does not allow the computation of ROM solutions with errors below a prescribed level, that is, "certified solutions" in the ROM modelling nomenclature. This is tightly linked to the sampling issue, that is, for what parameter values the snapshots should be computed to achieve this targeted error level. This issue is addressed by the certified Reduced Basis (RB) method, in which the snapshots are recursively computed by a Greedy Algorithm to progressively reduce the

* Corresponding author.
E-mail addresses: abandera@us.es (A. Bandera Moreno), ccaravaca@us.es (C. Caravaca García), chacon@us.es (T. Chacón Rebollo), edelgado1@us.es (E. Delgado Ávila), macarena@us.es (M. Gómez Mármol).

https://doi.org/10.1016/j.cma.2023.116683
Received 31 July 2023; Received in revised form 20 November 2023; Accepted 3 December 2023
Available online 8 December 2023

errors. This procedure needs a fast a posteriori error estimation (cf. [1,3,11]). Is has been applied to incompressible flows with increasing complexity: Stokes, Navier–Stokes and multi-parametric flows (cf. [12–16]). Moreover, some error indicators based on the dual norm of the discrete time-averaged residual have been used e.g. in [17,18] for the parameter selection in the Greedy Algorithm.

Kolmogorov's K41 energy cascade theory [19–23] is a fundamental concept in the field of fluid mechanics, and it provides a theoretical framework for understanding the energy transfer between different scales in a turbulent flow. In a fully developed turbulent flow, the kinetic energy is transferred from the large-scale eddies to smaller and smaller scales through a series of nonlinear interactions until it reaches the smallest scales, where it is dissipated into heat. This process is known as the energy cascade, and it is characterized by a self-similar scaling behaviour in the inertial subrange of scales. Kolmogorov's theory provides a statistical description of turbulence that has been widely used to guide the development of turbulence models and numerical simulations of turbulent flows.

The energy cascade concept has lead to the use of the high-order modes of the POD expansion to model the small scales within the inertial range. However a very large number of modes is needed to achieve a good precision, letting the ROM to need computing times similar to a Direct Numerical Simulation (DNS) solver (cf. [24,25]).

A way to build ROM model for turbulent flows consists in initially building a ROM for Navier–Stokes equations, and then model the unresolved scales (either by eddy diffusion or other techniques) to build the turbulence model. This approach has been followed in [26,27], for instance, where authors consider a VMS method to model the effect of the high order POD modes not considered in the ROM. Also in [28,29], authors propose a regularization for ROMs of the quasi-geostrophic equations to increase accuracy when the POD modes retained to construct the reduced basis are insufficient to describe the system dynamics, considering a linear differential filter for the vorticity. Moreover, ROM closures have been approximated by non-intrusive approaches instead of the classical Galerkin-POD procedure in [30–32]. An alternative strategy is to build ROMs for well-established turbulence models, actually here we address Large Eddy Simulation (LES) models. We already assume that the Smagorinsky turbulence model provides accurate enough solutions to turbulent flows with turbulence in statistical equilibrium. Our purpose is not to perform any kind of direct turbulence modelling with our reduction procedure, as intend the above mentioned techniques.

Certified RB LES Smagorinsky models for steady flows have been built with high computing speed-ups for single and multi-parametric configurations (cf. [33–36]). The error certification is based upon a posteriori error estimation procedures, that in their turn are built by the Brezzi–Rappaz–Raviart theory of approximation of regular branches of non-linear PDEs (cf. [37]), thanks to the enhanced regularity of the solutions of the Smagorinsky model. However, this procedure faces severe limitations. Indeed, the building of a posteriori error indicators is closely linked to the actual turbulence model and the actual FOM used, as well as to the nature of the parameters (either physical or geometrical) to deal with in the ROM. Actually, there is a well established theory for the Smagorinsky turbulence model (that possibly can be extended to more general LES models), based upon the improved regularity (w.r.t. Navier–Stokes equations) generated by the eddy viscosity term. This allows the construction of a-posteriori error estimation (cf. [34]), although these are highly computing time consuming, as stability factors in space–time should be computed and, in addition, depend on the discretization parameters.

In this paper we afford the building of a RB method for general transient LES parametric turbulence models, regardless of the FOM used. The basic tool is an error indicator based upon the physics of turbulent flows, rather than on the mathematics used to analyse the models. This error indicator measures the deviation of the energy spectrum of a trial solution versus the theoretical $k^{-5/3}$ spectrum predicted by the K41 theory of turbulence in statistical equilibrium.

In practice, this indicator leads to a stagnation of the Greedy Algorithm, that selects again a parameter already chosen. When stagnation occurs, we use a correction of this indicator, now measuring the deviation of the spectrum of the trial solution versus the spectrum of the reduced solution obtained in the current reduced basis. Indeed, the ROM solution is intended to approximate the FOM solution, whose spectrum already may have some error with respect to the theoretical K41 spectrum. In this correction of the error indicator, the reduced solution computed with the current reduced basis is used as a surrogate of the FOM solution.

To validate this indicator, on one hand we perform an error analysis on the basis of the K41 theory. This analysis proves that for isotropic flows the error between the FOM and ROM solutions of the Smagorinsky turbulence model is driven by the approximation error on the reduced space, plus the introduced energy spectrum-based error indicator. We further address some academic tests for the Smagorinsky turbulence model. We consider 2D periodic flows, yet meaningful, as they are designed to present the inertial spectrum predicted by the K41 theory. We assume that the Smagorinsky flow already has a part of its spectrum within the inertial range. The Empirical Interpolation Method (EIM) is used to compute reduced approximations of the non-linear eddy viscosity term [11,38,39]. We use two different POD filtering strategies to reduce the time snapshots. The Fast Fourier Transform (FFT) is used to compute the spectrum of the trial solutions. We compare the errors obtained with this strategy (using the error indicator) versus those obtained with the "optimal" error indicator, that is, the exact error. As a result, we obtain errors between the ROM and the FOM solutions quite close to the optimal ones. Further, we obtain a spectral decay of the error as the dimension of the reduced basis space increases, quite close to the one obtained if the exact error is used as indicator. We obtain speed-up rates of computing times of nearly 18.

The paper is structured as follows. In Section 2, we introduce error indicator based upon the K41 theory and state the combined Greedy Algorithm-POD strategy to build the reduced basis from this indicator. In Section 3, we recall the unsteady Smagorinsky turbulence model. In Section 4 we present the error analysis on the basis of the K41 theory, where the proofs of the results can be found in Appendix. The numerical tests are presented in Section 5. Finally, we present in Section 6 the conclusions of this work and its extension to more complex situations.

2. Reduced basis modelling of turbulent flows based on the statistical turbulence theory

The main purpose behind this section is the introduction of an *a posteriori* error indicator for turbulent flows. This *a posteriori* error indicator will allow us to select the parameter in the Greedy procedure for the construction of the reduced basis model.

For the development of this indicator, we have used general results from the Kolmogorov's K41 theory of turbulence in statistical equilibrium [21]. The main assumption behind this indicator is that the difference between the energy spectrum of a certain trial velocity field and the theoretical spectrum predicted by this theory is small for accurate solutions.

2.1. A posteriori error indicator based on the statistical turbulence theory

Andrei Kolmogorov stated in [21] that under suitable similarity and isotropy assumptions for turbulent flow in statistical equilibrium, there exists an inertial range $[k_1, k_2]$ in which, the turbulence energy spectrum $E(k)$ can be expressed in terms of the turbulent viscous dissipation ϵ and the wavenumber k.

For a high fidelity solution we can assume that, in the inertial subrange, this physical property accurately follows the expression

$$E(k, \mathrm{Re}) = \alpha(\mathrm{Re}) k^{-5/3}, \tag{1}$$

where $\alpha(\mathrm{Re}) > 0$ is a positive function depending on the turbulent dissipation ϵ of the solution for the Reynolds number, Re. It is fair to assume that the spectrum of the solution of the full-order model closely follows (1), as the full-order model is assumed to approximate the continuous problem faithfully in the resolved part of the inertial spectrum.

For a reduced trial velocity field that belongs to a reduced space of dimension N, we will denote by $E_N(k; \mathrm{Re})$ its energy spectrum. Bearing this into mind, we can define the *a posteriori* error indicator as follows,

$$\Delta_N(t; \mathrm{Re}) = \min_{\alpha \in \mathbb{R}} \left(\int_{k_1}^{k_2} \left| E_N(t, k; \mathrm{Re}) - \alpha(t; \mathrm{Re}) k^{-5/3} \right|^2 dk \right)^{1/2}. \tag{2}$$

This quantity measures the deviation between the spectrum of a reduced trial velocity at a given time and the theoretical spectrum in the inertial range $[k_1, k_2]$ described by the theory. In practice, we substitute k_2 by $k_c < k_2$, where k_c is the smallest scale we can solve numerically by means of the turbulence model considered. In most cases, k_c is related to the mesh size δ.

For the practical computation of the error estimator, we deal with the Discrete Fourier Transform (DFT). For this, let $\Omega \in \mathbb{R}^d$ be a square domain of length s. We divide each edge in m intervals of length $h = m/s$, with $m \in \mathbb{N}$ pair. Thus, considering $\mathbf{u} : \Omega \to \mathbb{C}$ a periodic velocity field (either FOM velocity or ROM velocity field), we consider for a Fourier mode $\mathbf{k} = (k_1, k_2)$, $k_1, k_2 = -s/2, -s/2 + 1, \dots, s/2$, the Discrete Fourier Transform, defined as:

$$\hat{\mathbf{u}}_{k_1 k_2} = \frac{1}{(s+1)^d} \sum_{j_1, j_2 = -s/2}^{s/2} \mathbf{u}(j_1 h, j_2 h) \bar{\phi}_{k_1 k_2}(j_1 h, j_2 h),$$

where $\bar{\phi}_{k_1 k_2}(j_1 h, j_2 h) = e^{2\pi i h (k_1 j_1 + k_2 j_2)}$. For a faster computation of the DFT, we use the Fast Fourier Transform (FFT) based upon a decomposition in terms of a Vandermonde matrix $\mathbb{F} \in \mathcal{M}^{(s+1)\times(s+1)}(\mathbb{C})$.

The total energy of the system $E(k, \mathrm{Re})$ (either for the FOM or ROM solution), can be approximated by

$$\int_0^\infty E(k, \mathrm{Re}) \approx \sum_{l=0}^{L_s} \sum_{l \le |\mathbf{k}| \le l+1} \frac{1}{2} |\hat{\mathbf{u}}_{\mathbf{k}}|^2,$$

where L_s is the integer part of $\sqrt{2}s$. Finally, the minimization over $\alpha \in \mathbb{R}$ is performed in practice by looking for the minimum value over a partitioned discrete interval $\Lambda \subset \mathbb{R}$.

Since the K41 theory is valid within the inertial spectrum, special care should be taken in the construction of the mesh $\mathcal{T}_h$ to compute the FOM, so we are effectively solving a part $[k_1, k_c]$ of the inertial spectrum.

The main advantage of this error estimator is that it can be applied no matter the numerical discretization and the turbulence model we are working with, as it only involves the spectrum of the trial solution. The only requirement is that the FOM accurately solves a part of the inertial spectrum. This avoids the construction of ad hoc *a posteriori* error estimators for the Reduced Basis discretization.

2.2. General algorithms to build the reduced basis spaces

In this section, we describe a general algorithm based on the *a posteriori* error indicator $\Delta_N(\mathrm{Re})$, presented in (2), for the construction of the reduced basis model of LES turbulent model. It is an adaptation of the standard combined Greedy-POD algorithm for the reduction of parametric flow problems. We describe it here for general LES FOM solvers. We particularize it to the Smagorinsky turbulence model in the next section.

We intend to solve parametric turbulent flows depending on a parameter $\mu \in \mathbb{R}^p$, for any integer $p \ge 1$. In the applications that follow this parameter will be the Reynolds number, although it can also be a different physical or geometrical parameter, or a multi-parameter, combination of these. We shall suppose that μ ranges on a compact set $D \subset \mathbb{R}^p$.

The general algorithm for the basis functions selection can be summarized as follows:

1. First, we determine a partition, $\mathcal{D}_{train}$, of the parameter space, $\mathcal{D}$, such that $\mathcal{D}_{train} \subset \mathcal{D}$. We also need to set the stopping criteria, and select an initial parameter $\mu_0^* \in \mathcal{D}_{train}$.
2. For a given reduced space, solve the full-order turbulence model at the different time steps (compute the snapshots), for the targeted time range $[t_1, t_L]$ and store the results of the velocity and pressure. It is needed that at the initial time, t_1 the turbulence is already at statistical equilibrium.
3. Apply some technique to compress the snapshots for the velocity and pressure, and add the compressed snapshots to the previous velocity and pressure Reduced Basis spaces.
4. Compute the *a posteriori* error indicator $\Delta_N(\mu)$ for each $\mu \in \mathcal{D}_{train}$ associated to the reduced basis. The error indicator should be computed for some discrete time sets to be determined.
5. Select the new parameter μ^* according to an appropriate criterium based upon the error indicator Δ_N (see Section 2.3 below).
6. Check the stopping criteria. If the criteria are fulfilled, then stop the algorithm, otherwise, repeat from step 2.

2.3. Criteria for the selection of new parameter values

Taking into account that we build the reduced solutions from the FE approximations, the indicator $\Delta_N(\mu)$ is not expected to vanish as N grows. Instead, it is expected to converge to the indicator for the solution of the full order model $\Delta_h(\mu)$, that is, to

$$\Delta_h(t;\mu) = \min_{\alpha\in\mathbb{R}} \left(\int_{k_1}^{k_c} |E_h(t,k;\mu) - \alpha(t;\mu)k^{-5/3}|^2 \, dk \right)^{1/2}$$

where $E_h(t,k;\mu)$ denotes the spectrum of the full-order solution for the resolved part of the inertial range $[k_1, k_c]$ at time t. This spectrum should be close to the theoretical $k^{-5/3}$ law if the FOM is accurately but, however, some error is to be expected as the FOM is not exact.

Then, the usual criterium for the selection of the best parameter in the Greedy algorithm, that is $\mu^* = \max_{\mu\in\mathcal{D}} \Delta_N(\mu)$, is no longer useful as it will not decrease to zero as N increases. Instead, we propose in Algorithm 1 new criteria for the selection of the next parameter at each step. Algorithm 1 first aims to add to the basis the information of the solutions whose energy spectrum is farther away from the theoretical one, then, if the parameter selected that way has been already selected in a previous iteration, we select between the non-selected parameters, the one that provides the largest difference between the energy spectrums of the previous and the current reduced solutions. In the latter case, we are assuming that the reduced error indicator $\Delta_N(\mu)$ is getting close to $\Delta_h(\mu)$, and the previous solution plays the role of the FOM one to compare with it.

We will compute the value of the indicator at the final time t_L, since the error with respect to the FOM solution is expected to increase as time increases.

Algorithm 1 Parameter selection criteria

Let S_N be the set of previously selected parameters.
Compute $\mu_N^* = \arg\max_{\mu\in\mathcal{D}train} \Delta_N(\mu, t_L)$;
if $\mu_N^* \in S_N$ **then**
  $\mu_N^* = \arg\max_{\mu\in\mathcal{D}train\setminus S_N} |\Delta_N(\mu, t_L) - \Delta_{N-1}(\mu, t_L)|$;
end if

2.4. Determination of new reduced space

In this section, we specify the procedure for the construction of the reduced spaces, actually we follow a procedure that combines two techniques, POD and Greedy, the so-called POD+Greedy approach [40].

In this procedure, we consider the time as a parameter for a separated POD strategy, while the Greedy procedure is applied on the parameter space. We solve the high-fidelity problem for a parameter value μ^*, and we perform a POD, for velocity and pressure separately, for the selected time snapshots. Then, we will select the next parameter value μ^* with the *a posteriori* error indicator criteria by means of a Greedy algorithm.

This procedure is described as follows:

1. Solve the full-order LES model for a given parameter, μ^*, for any discretization time t_n for $n = 1, \dots, L$. Select a POD procedure (see Section 5.2 for more details) given tolerance ϵ for the obtainment of the new reduced velocity and pressure spaces Y_N and M_N, respectively.
2. In order to assure that the inf–sup condition is satisfied for the pair of reduced velocity and pressure spaces, compute the inner pressure *supremizer* for the basis of the pressure resulting from the previous step (*cf.* [13]), and append it to the basis of the reduced velocity space (see Section 3.2 for a detailed description). If some stabilization techniques are considered (see e.g. [12,35]) this step would be no longer needed to be taken into account.
3. Finally, obtain the new parameter μ^* by applying the selection criteria presented in Algorithm 1 to the solutions of the reduced problem associated to the spaces Y_N and M_N.

3. Smagorinsky turbulence model

In this section, we focus on the development of the reduced LES turbulence model that we shall use to test the error indicator introduced in Section 2. Actually, we present the LES Smagorinsky model, that uses the K41 energy spectrum to model, in terms of eddy viscosity, the effect of the unresolved scales on the resolved ones [20]. We consider a finite element discretization, with an inf–sup stable pair of velocity–pressure spaces.

3.1. Full order model

For simplicity of notation, we present the Smagorinsky model as a continuous one, although it is intrinsically discrete, associated to a given discretization grid. We just specify its dependency on the actual grid used in the expression of the eddy viscosity terms. We thus consider a polygonal (when $d = 2$) or polyhedric (when $d = 3$) bounded domain $\Omega \subset \mathbb{R}^d$ and a triangular mesh $\{\mathcal{T}_h\}_{h>0}$ of Ω, that we assume to be regular in the sense of Ciarlet [41].

We consider that our model depends on one parameter, the Reynolds number, denoted by $\mu \in \mathcal{D}$, where $\mathcal{D}$ is an interval of positive real numbers, large enough to ensure that the flow is in well-developed turbulent regime.

Given a targeted final time T_f, we look for a velocity and pressure fields, $\mathbf{u} : \overline{\Omega} \times [0, T_f] \mapsto \mathbb{R}^d$, and $p : \overline{\Omega} \times [0, T_f] \mapsto \mathbb{R}$, respectively, such that verify

$$\begin{cases} \partial_t \mathbf{u} + \mathbf{u} \cdot \nabla \mathbf{u} + \nabla p - \nabla \cdot \left(\left(\frac{1}{\mu} + \nu_T(\mathbf{u}) \right) \nabla \mathbf{u} \right) = \mathbf{f} & \text{in } \Omega \times [0, T_f], \\ \nabla \cdot \mathbf{u} = \mathbf{0} & \text{in } \Omega \times [0, T_f]. \end{cases} \tag{3}$$

where $\mathbf{f}$ denotes the kinetic momentum source. The term $\nu_T(\mathbf{u})$ stands for the eddy viscosity, given by

$$\nu_T(\mathbf{u}) := \nu_T(\mathbf{u}, h) = C_S^2 \sum_{K \in \mathcal{T}_h} h_K^2 \left| \nabla \mathbf{u}_{|_K} \right| \chi_K, \tag{4}$$

where C_S denotes the Smagorinsky constant, h_K denotes the diameter of element K, and $\left| \cdot \right|$ denotes the Frobenius norm in $\mathbb{R}^{d \times d}$.

Model (3) should be completed with suitable initial and boundary conditions. We look for velocity $\mathbf{u}$ and pressure p in suitable spaces $Y \subset H^1(\Omega)^d$ and $M \subset L_0^2(\Omega)$, respectively, that take into account the essential boundary conditions.

To state the discretization of model (3), we consider two internal approximations, Y_h and M_h, of the spaces Y and M, respectively. To guarantee the well-posedness of discrete problem, we assure that these spaces satisfy the discrete uniform inf–sup condition,

$$\|q_h\|_{0,2,\Omega} = \sup_{\mathbf{v}_h \in Y_h} \frac{(q_h, \nabla \cdot \mathbf{v}_h)_\Omega}{\|\nabla \mathbf{v}_h\|_{0,2,\Omega}}, \quad \forall q_h \in M_h. \tag{5}$$

We consider the following Galerkin discretization of the unsteady Smagorinsky model (3),

$$\begin{cases} \forall \mu \in \mathcal{D}, t \in [0, T_f], \text{find } (\mathbf{u}_h(t;\mu), p_h(t;\mu)) \in Y_h \times M_h \text{ such that} \\ \left(\frac{\partial}{\partial t} \mathbf{u}_h, \mathbf{v}_h \right)_\Omega + a(\mathbf{u}_h, \mathbf{v}_h; \mu) + a_S(\mathbf{u}_h; \mathbf{u}_h, \mathbf{v}_h; \mu) \\ + b(\mathbf{v}_h, p_h; \mu) + c(\mathbf{u}_h, \mathbf{u}_h, \mathbf{v}_h; \mu) = \langle \mathbf{f}, \mathbf{v}_h \rangle & \forall \mathbf{v}_h \in Y_h, \\ b(\mathbf{u}_h, q_h; \mu) = 0 & \forall q_h \in M_h. \end{cases} \tag{6}$$

Here, $a(\cdot, \cdot; \mu)$ and $b(\cdot, \cdot; \mu)$ are bilinear forms defined as

$$a(\mathbf{u}, \mathbf{v}; \mu) = \frac{1}{\mu} \int_\Omega \nabla \mathbf{u} : \nabla \mathbf{v} \, d\Omega, \qquad b(\mathbf{v}, q; \mu) = -\int_\Omega (\nabla \cdot \mathbf{v}) q \, d\Omega. \tag{7}$$

Also, $c(\cdot, \cdot, \cdot; \mu)$ is a trilinear skew-symmetric form, given by

$$c(\mathbf{z}, \mathbf{u}, \mathbf{v}; \mu) = \frac{1}{2} \left[\int_\Omega (\mathbf{z} \cdot \nabla \mathbf{u}) \mathbf{v} \, d\Omega - \int_\Omega (\mathbf{z} \cdot \nabla \mathbf{v}) \mathbf{u} \, d\Omega \right]. \tag{8}$$

Finally, $a_S(\cdot; \cdot, \cdot; \mu)$ is a non-linear form that models the eddy viscosity effects, stated as

$$a_S(\mathbf{z}; \mathbf{u}, \mathbf{v}; \mu) = \int_\Omega \nu_T(\mathbf{z}) \, \nabla \mathbf{u} : \nabla \mathbf{v} \, d\Omega. \tag{9}$$

If the inf–sup condition (5) is satisfied by the pair of finite element velocity–pressure spaces, Y_h and M_h, problem (6) is well-posed: it admits a solution which is bounded in natural norms in terms of the norms of the data. We do not precise the actual bounds as these are not necessary for our derivation. See [20] for more details.

3.2. Reduced basis model

We next formulate the Reduced Basis model for the Smagorinsky model (3). This is also a Galerkin projection of the Smagorinsky model, but now the projection is performed onto the reduced basis spaces, with much lower dimension. It reads $\forall \mu \in \mathcal{D}$ and $t \in [0, T_f]$, find $(\mathbf{u}_N(t;\mu), p_N(t;\mu)) \in Y_N \times M_N$ such that

$$\begin{cases} \left(\frac{\partial}{\partial t}\mathbf{u}_N, \mathbf{v}_N\right)_\Omega + a(\mathbf{u}_N, \mathbf{v}_N; \mu) + a_S(\mathbf{u}_N; \mathbf{u}_N, \mathbf{v}_N; \mu) \\ +b(\mathbf{v}_N, p_N; \mu) + c(\mathbf{u}_N, \mathbf{u}_N, \mathbf{v}_N; \mu) = \langle \mathbf{f}, \mathbf{v}_N \rangle & \forall \mathbf{v}_N \in Y_N, \\ b(\mathbf{u}_N, q_N; \mu) = 0 & \forall q_N \in M_N; \end{cases} \tag{10}$$

where Y_N and M_N respectively denote the reduce velocity and pressure spaces. The construction of those spaces is performed following POD+Greedy procedure explained in Section 2.4.

We assume that the family of pairs of reduced spaces $\{(Y_N, M_N),\ N = 1, 2, \dots\}$ satisfies the discrete inf–sup condition (5). This may be achieved adding to the reduced velocity space obtained from the POD-Greedy algorithm the supremizers of a basis of the reduced velocity space M_N (see e.g. [10,13]). The inner pressure supremizer of $q_N \in M_N$ is given by

$$T_p^\mu q_N \in Y_h \text{ such that } \left(\nabla T_p^\mu q_N, \nabla \mathbf{v}_h\right)_\Omega = b(q_h, \mathbf{v}_h; \mu) \quad \forall \mathbf{v}_h \in Y_h. \tag{11}$$

Once the reduced inf–sup condition is ensured, problem (10) is also well-posed, much as the finite element problem (6) is (see eg. [20]). We use this enrichment of the reduced velocity space to stabilize the reduced pressure discretization in our numerical experiments.

To build the POD correlation matrices, for velocity and pressure, we consider the natural norms for velocity and pressure spaces, that is, the H^1-seminorm for the velocity space, and the L^2-norm for the pressure space.

The eddy viscosity term defined in (4), $\nu_T(\mathbf{u}(\mu))$, is a non-linear function of the parameter. This kind of non-linearities are commonly treated on the ROM benchmark by tensorizing them in the offline phase. With this purpose, we use the Empirical Interpolation Method (EIM) [11,38,39]. We define a reduced basis space $W_M^S = \text{span}\{\psi_1^S, \dots, \psi_M^S\}$ to approximate the variety of eddy viscosity terms, $\{\nu_T(\mathbf{u}(\mu))\}_{\mu \in \mathcal{D}}$. This reduced basis space is also constructed by selecting the parameter values with a Greedy algorithm during the EIM procedure, in which we consider both the time and the Reynolds number as parameters. With the EIM, we approximate the Smagorinsky eddy diffusion form by a tensorized expression,

$$a_S(\mathbf{u}_N, \mathbf{v}_N; \mu) \approx \tilde{a}_S(\mathbf{u}_N, \mathbf{v}_N; \mu) = \sum_{k=1}^{M} \sigma_k^S(\mu) s(\psi_k^S, \mathbf{u}_N, \mathbf{v}_N), \tag{12}$$

with

$$s(\psi_k^S, \mathbf{u}_N, \mathbf{v}_N) = \sum_{K \in \mathcal{T}_h} \left(\psi_k^S \nabla \mathbf{u}_N, \nabla \mathbf{v}_N\right)_K. \tag{13}$$

In the numerical experiments, we actually solve the RB problem (10) considering the tensorized form $\tilde{a}_S(\cdot, \cdot; \mu)$ instead of the original one $a_S(\cdot; \cdot, \cdot; \mu)$.

4. Error estimates

We provide in this section some arguments aimed at justifying, on physical and mathematical grounds, why the K41-based error estimator provides accurate ROM solutions of the Smagorinsky turbulence models. In [20], Chapter 5, it is proved that the turbulent dissipation ε satisfies

$$\varepsilon = \frac{1}{\mu} \int_0^\infty k^2 E(k)\, dk, \quad \overline{|D(\mathbf{u})|}^2 = \frac{\mu}{2} \varepsilon, \tag{14}$$

where $D(\mathbf{u})$ denotes the symmetric gradient, that is, $D(\mathbf{u}) = 1/2(\nabla \mathbf{u} + \nabla \mathbf{u}^T)$.

The Smagorinsky turbulence model is built assuming that the eddy viscosity is expressed in terms of the cutoff length (identified with the grid size h) and the gradient of the resolved (large scale) velocity $\overline{\mathbf{u}}$, by (cf. [20], Chapter 5, Section 5.5)

$$\nu_T(\overline{\mathbf{u}}) = C\, h^2\, |D\overline{\mathbf{u}}|, \tag{15}$$

where for brevity we drop the dependence of $\overline{\mathbf{u}}$ w.r.t $\mathbf{x}$ and t. Based upon (14), it is also assumed that it holds

$$|D\overline{\mathbf{u}}|^2 = \frac{1}{2} \int_{k_1}^{k_c} k^2 E(k)\, dk \tag{16}$$

where $[k_1, k_c]$ is the part of the inertial spectrum within the resolved flow, assuming $k_1 \ll k_c$. Note that $k_c \approx 1/h$.

In the following proposition, we give an upper bound for the difference of the turbulent viscosities of two velocity fields of locally isotropic flows.

Proposition 1. *Assuming (16) holds, if $\mathbf{u}_1$ and $\mathbf{u}_2$ are the velocity fields of two locally isotropic flows, it follows that*

$$|\nu_T(\mathbf{u}_1) - \nu_T(\mathbf{u}_2)| \le C\, h^2 \left(\int_{k_1}^{k_c} k^2\, |E(k)(k; \mathbf{u}_1) - E(k)(k; \mathbf{u}_2)|\, dk \right)^{1/2}, \tag{17}$$

where we denote by $E(k)(k; \mathbf{u})$ the energy spectrum of velocity $\mathbf{u}$. Furthermore, if $|E(k)(\mathbf{u}_1) - E(k)(\mathbf{u}_2)| \le \delta, \forall k \in [k_1, k_c]$, then

$$|\nu_T(\mathbf{u}_1) - \nu_T(\mathbf{u}_2)| \le C(\delta h)^{1/2}. \tag{18}$$

The proof can be consulted in the Appendix.

Thanks to Proposition 1, we can state the following theorems about the error bounds of the solutions of turbulent problems. We shall denote by ν_e the minimum "effective" viscosity, defined in the following. The sketch of the proof of the following theorem can be consulted in the Appendix.

In the sequel, we denote by C a constant that may vary from line to line, but that is always independent on ν and the discretization parameters h and Δt. Moreover, we denote by $\|\cdot\|_{n,p}$ the norm of the $W^{n,p}(\Omega)$ space and, for simplicity, we denote $\|\cdot\|_p = \|\cdot\|_{0,p}$. With base on Proposition 1, we obtain

Theorem 2. *Let $\mathbf{u}_1, \mathbf{u}_2$ be two velocity fields of locally isotropic flows, solution of the Smagorinsky turbulence model (3). Assuming that $|E(k)(\mathbf{u}_1) - E(k)(\mathbf{u}_2)| \leq \delta, \forall k \in [k_1, k_c]$ and that $\mathbf{u}_1, \mathbf{u}_2 \in L^\infty(W^{1,3})$, we obtain the following error bound*

$$\|\boldsymbol{r}(t)\|_2^2 + \nu_e \int_0^t e^{\frac{C}{\nu_e}(t-s)} \|\nabla \boldsymbol{r}(s)\|_2^2 ds \leq e^{\frac{C}{\nu_e}t} \|\boldsymbol{r}(0)\|_2^2 + \frac{C}{\nu_e} h\delta (e^{\frac{C}{\nu_e}t} - 1), \tag{19}$$

where $\boldsymbol{r} = \mathbf{u}_1 - \mathbf{u}_2$, and ν_e is the minimum effective viscosity for any of the velocity fields,

$$\nu_e = \nu + (C_S\, h)^2 \max \left\{ \inf_{\Omega \times [0,T]} |\nabla \mathbf{u}_1|, \inf_{\Omega \times [0,T]} |\nabla \mathbf{u}_2| \right\}.$$

The main steps of the proof of this result are given in Appendix.

For the following theorem, we denote by $\boldsymbol{w}_N$ the projection of $\mathbf{u}_h$ into the reduced space, and $\boldsymbol{\rho}_N = \boldsymbol{w}_N - \mathbf{u}_h$. The proof of this theorem follows the same ideas as Theorem 2 but considering $\mathbf{u}_h$ and $\mathbf{u}_N$ instead of $\mathbf{u}_1$ and $\mathbf{u}_2$. For a sketch of the proof, see Appendix.

Theorem 3. *Let $\mathbf{u}_h$ be the solution of the FOM Smagorinsky model (6) and $\mathbf{u}_N$ the solution of ROM Smagorinsky model (10). Assume that*

$$|E(k)(\mathbf{u}_h) - E(k)(\mathbf{u}_N)| \leq \delta, \forall k \in [k_1, k_c].$$

Then, the following error estimate holds

$$\begin{aligned} &\|\boldsymbol{e}_N(t)\|_2^2 + \nu_e \int_0^t \exp(\sigma(s) - \sigma(t)) \|\nabla \boldsymbol{e}_N(s)\|_2^2 ds \leq \\ &\quad \|\boldsymbol{e}_N(0)\|_2^2 \exp(-\sigma(t)) + \int_0^t P_N(s) \exp(\sigma(s) - \sigma(t)) ds \\ &\quad + \frac{C}{\nu_e} h\delta \int_0^t \|\nabla \mathbf{u}_h(s)\|_2^2 \exp(\sigma(s) - \sigma(t)) ds, \end{aligned} \tag{20}$$

where $\boldsymbol{e}_N = \boldsymbol{w}_N - \mathbf{u}_N$, is the error between $\boldsymbol{w}_N$ and the reduced solution $\mathbf{u}_N$, ν_e is the minimum effective viscosity,

$$P_N = C\|\partial_t \boldsymbol{\rho}_N\|_2^2 + \frac{C}{\nu_e} \left(\nu + \|\nabla \mathbf{u}_h\|_2^2 + \|\nabla \boldsymbol{w}_N\|_2^2\right) \|\nabla \boldsymbol{\rho}_N\|_2^2 + \frac{C}{\nu_e} \|\nu_T(\mathbf{u}_h) \nabla \boldsymbol{\rho}_N\|_2^2,$$

is the term that includes all the approximation errors on the reduced space, and

$$\sigma_N(t) = C \left(t + \frac{1}{\nu_e} \left(\|\nabla \boldsymbol{w}_N\|_{L^2(L^3)}^2 + \|\boldsymbol{w}_N\|_{L^2(L^\infty)}^2 \right) \right).$$

Remark 1. By Theorem 2, the difference between two locally isotropic solutions of the Smagorinsky turbulence model is just driven by the deviation between their energy norms.

Remark 2. By Theorem 3, and assuming some results from K41 theory, we may explain the combined role of reduced basis interpolation and the a priori error estimation based upon energy spectrum. Note that using the inverse error estimates for finite element functions (cf. [20], Appendix)

$$\|\mathbf{u}_h\|_{m,p} \leq C\, h^{n-m+d/p-d/q} \|\mathbf{u}_h\|_{n,q}, \quad \text{if } n - m + d/p - d/q \leq 0,\ m \geq n,$$

it follows

$$|\nu_T(\mathbf{u}_h)| \leq C_S\, h^2 \|\nabla \mathbf{u}_h\|_\infty \leq C\, h^{1-d/2} \|\mathbf{u}_h\|_2 \leq C\, h^{1-d/2},$$

as the standard estimates for the Galerkin approximation of Smagorinsky equations prove that $\mathbf{u}_h$ is bounded in $L^\infty(L^2)$ by a bound independent of ν. Similarly,

$$\|\nabla \mathbf{u}_h\|_2 + \|\nabla \boldsymbol{w}_N\|_2 \leq C\, h^{-1} (\|\mathbf{u}_h\|_2 + \|\boldsymbol{w}_N\|_2) \leq C\, h^{-1} \|\mathbf{u}_h\|_2 \leq C\, h^{-1}.$$

Consequently,

$$P_N \leq C\, \|\partial_t \boldsymbol{\rho}_N\|_2^2 + \frac{C}{\nu_e} \left(\nu^2 + h^{-2}\right) \|\nabla \boldsymbol{\rho}_N\|_2^2.$$

Also,

$$\|\nabla \boldsymbol{w}_N\|^2_{L^2(L^3)} + \|\boldsymbol{w}_N\|^2_{L^2(L^\infty)} \leq C\, h^{-1+d/3-d/2} + h^{-d/2} \leq C\, h^{-1-d/6},$$

what implies

$$\exp(\sigma_N(t)) \leq \alpha(t,h) := C\, \exp\left(t + \frac{1}{\nu_e}\, h^{-2-d/3}\right).$$

Then, combining the last two estimates with (20),

$$\begin{aligned} &\|\boldsymbol{e}_N(t)\|_2^2 + \nu_e \int_0^t \|\nabla \boldsymbol{e}_N(s)\|_2^2 ds \leq \alpha(t,h)\, \|\boldsymbol{e}_N(0)\|_2^2 + \\ &\quad \alpha(t,h)\, \|\partial_t \boldsymbol{\rho}_N\|^2_{L^2(L^2)} + \frac{C}{\nu_e}\left(\nu^2 + h^{-2}\right) \|\nabla \boldsymbol{\rho}_N\|^2_{L^\infty(L^2)} \\ &\quad + \frac{C}{\nu_e}\, t\, \alpha(t,h)\, h^{-1}\, \delta, \end{aligned} \tag{21}$$

Let us assume that $\boldsymbol{w}_N$ accurately reproduces the large scales of $\mathbf{u}_h$ up to a wavenumber $k_N < k_c$. By analogy with hypothesis (16) it is reasonable to assume that (recall that $\boldsymbol{\rho}_N = \boldsymbol{w}_N - \mathbf{u}_h$)

$$|\nabla \boldsymbol{\rho}_N|^2 \simeq \frac{1}{2} \int_{k_N}^{k_c} k^2 E(k)\, dk \tag{22}$$

Assuming next that the K41 theory holds, this yields

$$|\nabla \boldsymbol{\rho}_N|^2 \simeq \frac{1}{2} \int_{k_N}^{k_c} k^2\, k^{-5/3}\, dk = \frac{2}{3}\ \left(k_c^{4/3} - k_N^{4/3}\right).$$

In numerical computations, $\partial_t \boldsymbol{\rho}_N$ is replaced by some discrete time derivative, and then

$$\|\partial_t \boldsymbol{\rho}_N\|^2_{L^2(L^2)} \leq C\Delta t^{-2} \|\boldsymbol{\rho}_N\|^2_{L^2(L^2)} \leq C\Delta t^{-2} \|\nabla \boldsymbol{\rho}_N\|^2_{L^2(L^2)}.$$

We then arrive at the error estimate

$$\begin{aligned} &\|\boldsymbol{e}_N(t)\|_2^2 + \nu_e \int_0^t \|\nabla \boldsymbol{e}_N(s)\|_2^2 ds \lessapprox \alpha(t,h)\, \|\boldsymbol{e}_N(0)\|_2^2 + \\ &\quad C\left(\alpha(t,h)\Delta t^{-2} + \frac{1}{\nu_e}\left(\nu^2 + h^{-2}\right)\right)\left(k_c^{4/3} - k_N^{4/3}\right) \\ &\quad + \frac{C}{\nu_e}\, t\, \alpha(t,h)\, h^{-1}\, \delta, \end{aligned} \tag{23}$$

where we identify k_c with h^{-1}.

Estimate (23) is a kind of a posteriori error estimate. The second term in this bound allows to estimate the number of POD modes needed to achieve a targeted impact in $\boldsymbol{e}_N$ due to approximation in the current reduced basis space. In its turn, the last term allows to estimate the accuracy δ needed to approximate the spectrum to achieve targeted error threshold in $\boldsymbol{e}_N$. Let us recall that the grid size h is given for an actual realization of the Smagorinsky model. If h is diminished, then the number of POD modes should increase and δ should decrease, according to the previous estimate.

This supports the use of this error estimator in the building of a reduced basis model for the Smagorinsky model.

5. Numerical tests

In this section, we will validate the behaviour of the estimator Δ_N. To do so, we consider two possible choices of the parameter set. Firstly we take the parameters obtained from the Greedy algorithm and secondly we consider a uniform partition within the range where the parameter.

We consider the domain $\Omega \times [0,T]$, with $\Omega = [-1/2, 1/2]^2$ and $T = 30$ and we solve the Smagorinsky model (6) for 2D periodic flows, with periodic boundary conditions and assume no external sources, thus $\mathbf{f} = 0$.

In order to obtain the approximate solution, we use a semi-discretization in time using the Crank–Nicolson method, and for the resolution of the resulting problem we use stable finite elements for the pressure velocity, specifically Taylor–Hood i.e., $\mathbb{P}2-\mathbb{P}1$. The mesh on which it is solved is a structured mesh, with $m = 64$ intervals in each of the directions, obtaining a mesh with 8192 triangles and 4225 vertices. The parameter considered is the Reynolds number μ, which we consider moves in the range $D = [1000, 16\,000]$. For this range, approximately a time greater than 10 is needed to reach the profile of the Kolmogorov spectrum. In this case there is no inertial spectrum k^{-3} of the 2D turbulence, as a consequence of no forcing at large wavenumbers (cf. [42]).

5.1. Data of the problem and initial condition

As an initial condition we will consider a velocity field with an energy spectrum of the form (1). This field is going to be constructed through the Fourier transform, as follows: we take $w_h^0 = (v, v)$ where v is such that its Fourier transform is given by

$$\hat{v}(k) = \begin{cases} k^{-(5/3+1)/2} & \text{if } 0 < k \leq m/4, \\ 0 & \text{other case.} \end{cases} \tag{24}$$

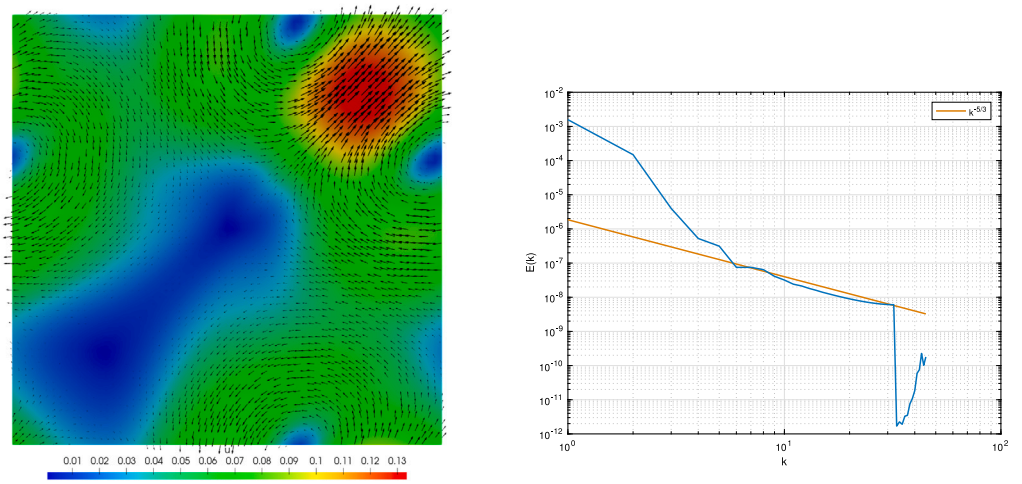

Fig. 1. Initial condition $\mathbf{u}_h^0$ and its energy spectrum.

Then, we define the initial condition $\mathbf{u}_h^0$ as the solution of the Smagorinsky model, for the mean value of the parameter, $\mu = 8500$, time half of the total, that is, $t = 15$, taking as initial condition for the problem (6), w_h^0.

In Fig. 1, we can see the initial condition u_h^0 constructed and its energy spectrum. We can observe that for wavenumbers k between 5 and 32 a good approximation of the initial spectrum is obtained. For values larger than $k_c = 32$, we see a sharp decay of the energy, because these wavenumbers are outside the circle of largest radius completely contained in the unit square and viscous effects.

5.2. Selection of the POD+Greedy procedure

In this subsection, we aim to select the method that we will be using in the following numerical study. For this part, and in the following, we will use the following combined velocity–pressure relative error

$$\epsilon_N(t;\mu) = \left(\frac{\|\mathbf{u}_h(t;\mu) - \mathbf{u}_N(t;\mu)\|_{H^1}^2 + \|p_h(t;\mu) - p_N(t;\mu)\|_2^2}{\|\mathbf{u}_h(t;\mu)\|_{H^1}^2 + \|p_h(t;\mu)\|_2^2} \right)^{1/2}. \tag{25}$$

From this definition, we focus on two quantities of interest: the error at the final time step, i.e. $\epsilon_N(T_f;\mu)$, and the time-integrated error, i.e. $\int_{t_0}^{T_f} \epsilon_N(t;\mu)dt$.

First, we will compare various POD+Greedy procedures existing in the literature. More precisely, we are comparing four approaches:

1. **Complete POD:** We store all the snapshots for every selected parameter and perform the POD to the complete snapshot matrix.
2. **Hierarchical POD:** We perform a POD to the snapshots corresponding to the last selected parameter and add the result to the previous reduced basis, so $Y_N \subset Y_{N+1}$, $M_N \subset M_{N+1}$. For more information about this procedure, see [43].
3. **Incremental HAPOD:** We perform a POD to the snapshots corresponding to the last selected parameter and add the result to the previous reduced basis, then perform a second POD to obtain the new reduced basis. For more information about this procedure, see [44].
4. **Reduced POD:** We add the snapshots corresponding to the last selected parameter to the previous reduced basis and perform a POD to obtain the new reduced basis.

In Fig. 2, we can see the comparison between the aforementioned methods in terms of the l_2 and l_∞ norms. The behaviour is similar in both norms, and we can conclude various things from this comparison. On the one hand, we can see that the Reduced POD approach outperforms the others but stagnates in a low dimension of the reduced basis with no further improvement. On the other hand, the complete POD provides a better approximation of the full-order solution for a higher dimension of the reduced basis, achieving almost two more orders of magnitude in the relative error. Taking this into account, we will be using the Complete POD procedure in the following study. In practice, the best strategy would be to use the Reduced POD until stagnation, and then use the Complete POD. For the sake of completeness, we present in Table 1 a comparison of the evolution of the l_2-norm of the relative errors for the same approaches. In this table, we can clearly see that the Complete POD approach outperforms the Reduced POD at each POD+Greedy iteration, and that after the sixth iteration the Reduced POD approach stagnates with a l_2-norm of the relative error equal to l_2-norm of the relative error.

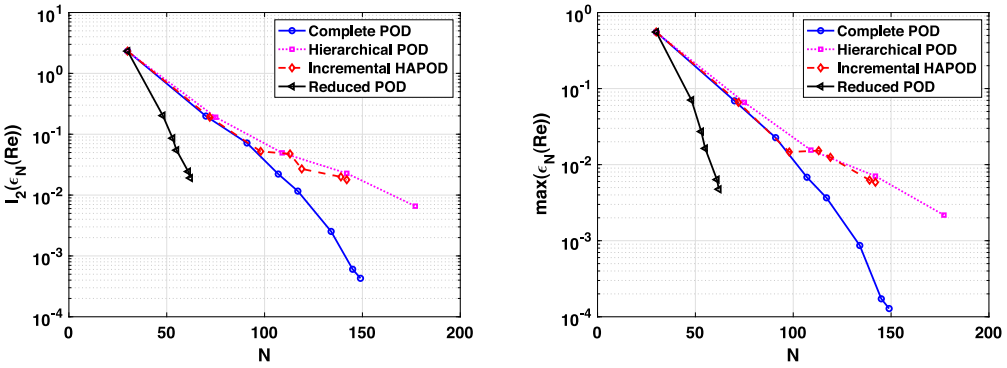

Fig. 2. Comparison of the performance of different POD+Greedy approaches with the use of the Kolmogorov error indicator. Left panel shows a comparison in parametric l_2-norm and right panel shows the comparison in parametric l_∞-norm. For both panels, on the x-axis stands for the dimension of the reduced space N, and on the y-axis stands for the relative error w.r.t the full-order solution in logarithmic scale.

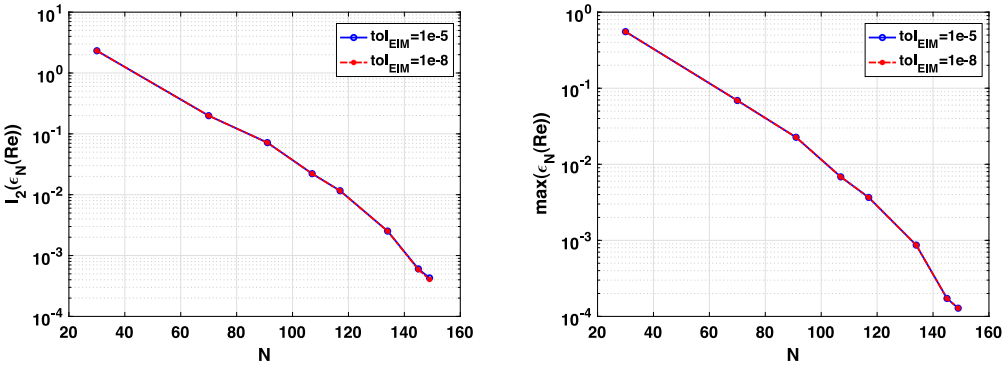

Fig. 3. Comparison of the performance of different EIM approaches with the use of the Kolmogorov error indicator. Left panel shows a comparison in parametric l_2-norm and right panel shows the comparison in parametric l_∞-norm. For both panels, the x-axis stands for the dimension of the reduced space N, and the y-axis stands for the relative error w.r.t the full-order solution in logarithmic scale.

Table 1
Comparison of the l_2-norm of the relative error at each iteration of the POD+Greedy algorithm for the Complete POD and Reduced POD approaches. We can see that after the sixth iteration, the l_2-norm for the Reduced POD approach stagnates.

It.	Complete POD	Reduced POD
1	$5,54 \cdot 10^{-1}$	$5,54 \cdot 10^{-1}$
2	$6,90 \cdot 10^{-2}$	$7,07 \cdot 10^{-2}$
3	$2,27 \cdot 10^{-2}$	$2,72 \cdot 10^{-2}$
4	$6,83 \cdot 10^{-3}$	$1,63 \cdot 10^{-2}$
5	$3,66 \cdot 10^{-3}$	$6,36 \cdot 10^{-3}$
6	$8,66 \cdot 10^{-4}$	$4,75 \cdot 10^{-3}$
7	$1,72 \cdot 10^{-4}$	$4,75 \cdot 10^{-3}$
8	$1,28 \cdot 10^{-4}$	$4,75 \cdot 10^{-3}$

The stagnation of the Reduced POD could be explained by the error term in estimate (23) stemming from the POD interpolation. Once the smallest scales of $\mathbf{u}_h$ are well reproduced by the ROM, this term nearly vanishes, as well as the one due to the approximation of the error spectrum. The Reduced POD extracts the dominant features of the FOM until the grid size scale. The remaining POD procedures give smaller errors with respect to the FOM solution, although possibly the scales smaller than the grid size are spurious, with no physical meaning, as the Smagorinsky model only accurately reproduces the large scales that can be represented in the grid.

5.3. Approximation of eddy viscosity term by EIM

In this subsection, we study the tensorization of the Smagorinsky turbulent viscosity (4) with respect to the parameter, for which we will use the EIM. To test the accuracy of this procedure, we will compare two settings:

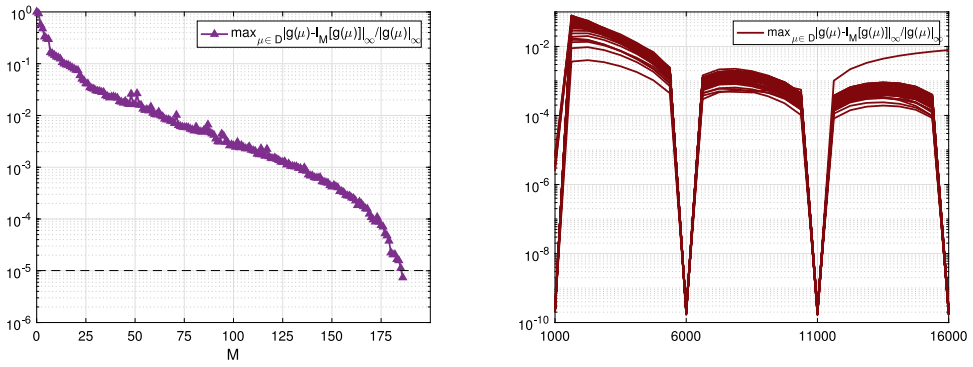

(a) EIM history convergence error. (b) EIM error at t_n for $n = 1, \ldots, L$.

Fig. 4. EIM error evolution.

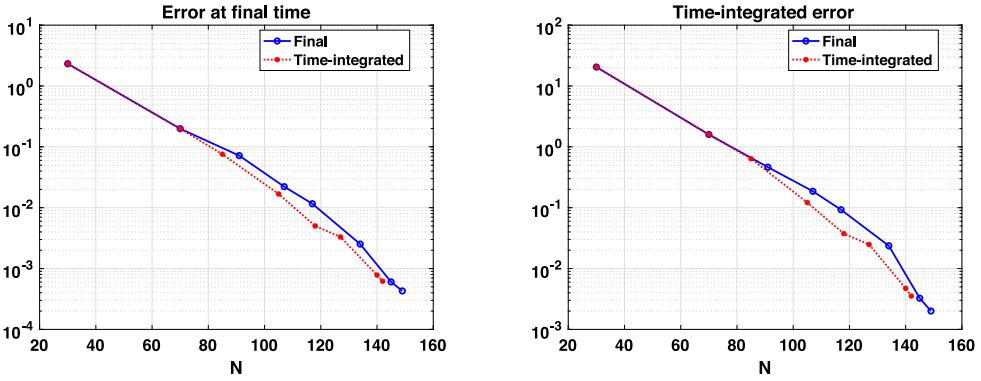

Fig. 5. Comparison of the performance of different approaches for the Kolmogorov error indicator. Left panel shows a comparison of the relative error at the final time and right panel shows the comparison of the parametric l_1-norm of the relative errors in time. For both panels, the x-axis stands for the dimension of the reduced space N, and the y-axis is in logarithm scale.

- On the one hand, we choose a set of 4 values of the parameter $\mu = \{1000, 6000, 11\,000, 16\,000\}$ and we calculate the finite element solution $(\mathbf{u}_h^n(\mu), p_h^n(\mu))$ for different time instants $n = 1, \ldots, L$. With these snapshots we calculated an approximation of the viscosity function, by EIM taking a tolerance of $\epsilon_{EIM} = 10^{-5}$, resulting in 186 basis functions.
- On the other hand, we choose a set of 25 equispaced values of the parameter, instead of 4 as in the previous setting, and reduce the tolerance to $\epsilon_{EIM} = 10^{-8}$. Following the same procedure as for the previous point, we obtain 723 basis functions.

The objective is to compare the results obtained by means of the EIM, considering that the second one is a highly accurate representation of the Smagorinsky turbulent viscosity term (4) and would act as if we were computing the Smagorinsky turbulent viscosity term in the original full-order space. We follow this approach, as computing the exact eddy viscosity would lead to very high computing times in the ROM.

In Fig. 3, we show a comparison of the error decay in parametric l_2 and l_∞ norms. It can be clearly seen that both decays are almost identical in both norms. Therefore, the first proposed EIM setting does not result on an augmentation of the error. So, in the following study, we will consider the first EIM setting.

For the sake of completeness, we present in Fig. 4(a) the convergence error of EIM as a function of the number of bases M, in Fig. 4(b), we see the error where each line corresponds to a time instant t_n for $n = 1, \ldots, 48$.

5.4. Treatment of time variability in the error indicator

The final matter that we need to address before the validation is if the use of the Kolmogorov error indicator at the final time step, i.e. $\Delta_N(T_f; \mu)$, is good enough for our purpose, or we need to use a time-integrated version of it , i.e. $\int_{t_0}^{T_F} \Delta_N(t; \mu) dt$. In order to tackle this question, we will perform a comparison between the use of the indicator at the final step and the use of the time-integrated indicator.

Table 2
Convergence story of the POD+Greedy algorithm with Complete POD, using $\Delta_N(\mu)$, the indicator, (upper table) and $\epsilon_N(\mu)$, the exact error, (lower table) for the parameter selection.

It.	μ	N	$\max_\mu \Delta_N(\mu)$	$\max_\mu \lvert\Delta_N(\mu) - \Delta_{N^*}(\mu)\rvert$	$\max_\mu(\epsilon_N(\mu))$
1	1000	30	$7,92 \cdot 10^{-1}$		$5,54 \cdot 10^{-1}$
2	16 000	70	$5,16 \cdot 10^{-1}$		$6,90 \cdot 10^{-2}$
3	1625	91	$3,53 \cdot 10^{-1}$		$2,27 \cdot 10^{-2}$
4	2250	107		$3,93 \cdot 10^{-2}$	$6,83 \cdot 10^{-3}$
5	2875	117		$1,79 \cdot 10^{-2}$	$3,66 \cdot 10^{-3}$
6	6000	134		$2,08 \cdot 10^{-3}$	$8,66 \cdot 10^{-4}$
7	12 875	145		$1,53 \cdot 10^{-3}$	$1,72 \cdot 10^{-4}$
8	10 375	149		$2,23 \cdot 10^{-4}$	$1,28 \cdot 10^{-4}$

It.	μ	N	$\max_\mu \epsilon_N(\mu)$
1	1000	30	$5,54 \cdot 10^{-1}$
2	16 000	70	$6,90 \cdot 10^{-2}$
3	3250	96	$1,34 \cdot 10^{-2}$
4	1625	111	$4,76 \cdot 10^{-3}$
5	8500	132	$7,54 \cdot 10^{-4}$
6	5375	141	$3,59 \cdot 10^{-4}$
7	12 875	147	$2,78 \cdot 10^{-4}$
8	2250	150	$1,23 \cdot 10^{-4}$

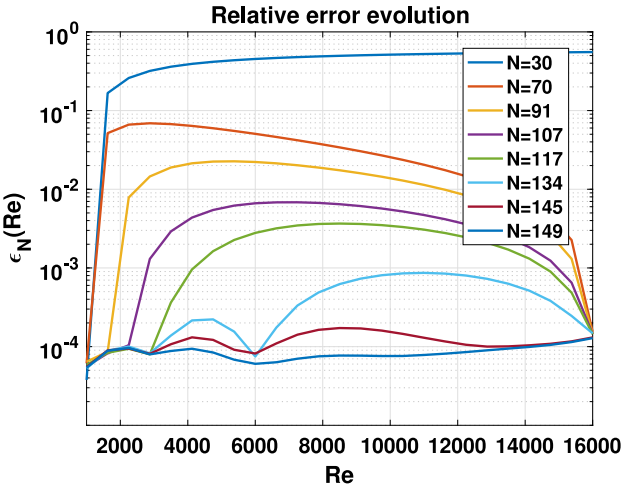

Fig. 6. Error $\epsilon_N(\mu)$ in each iteration of the POD+Greedy algorithm, using the Kolmogorov error indicator.

In Fig. 5, we can see the comparisons of error decay for both approaches. We can see that in both cases the error decay is quite similar, although the time-integrated approach provides a slightly better relative error. However, the gain of using the time-integrated version does not compensate the computational effort that has to be done in the offline stage. So, for the rest of the study, we will keep the use of the indicator at the final step.

5.5. Validation of the Kolmogorov error indicator

In this first test, we will validate the *a posteriori* error indicator $\Delta_N(\mu)$ introduced in (2), using the parameter values provided by the Greedy algorithm, that provides the best value of the parameter at each iteration, and we compare the indicator with the exact error for the final time $T_f = 30$.

Table 2, upper part, shows the errors between the reduced method solution and the FOM solution, using the indicator $\Delta_N(\mu)$. In the lower part, we present the exact errors for the selection of parameters chosen by the Greedy algorithm.

We are using as notation N the actual dimension of the reduced spaces $Y_N \times M_N$, instead of the iteration of the Greedy algorithm, although it is an abuse of notation, it is done for a better compression of the table.

Figs. 6 and 7 show the evolution of the relative errors, using the indicator and the exact error, respectively. As we can see, the relative errors for the different numbers of basis functions are similar. These figures have been obtained from Table 2 and we can see that in both cases for the last iterations the relative errors in the last iterations were of the same order 10^{-4}.

As mentioned above, the estimator $\Delta_N(\mu)$ is not expected to converge to 0 when the dimension N of the reduced space grows, rather it should converge to Δ_h, since the reduced solution is constructed from the finite element approximation. This convergence

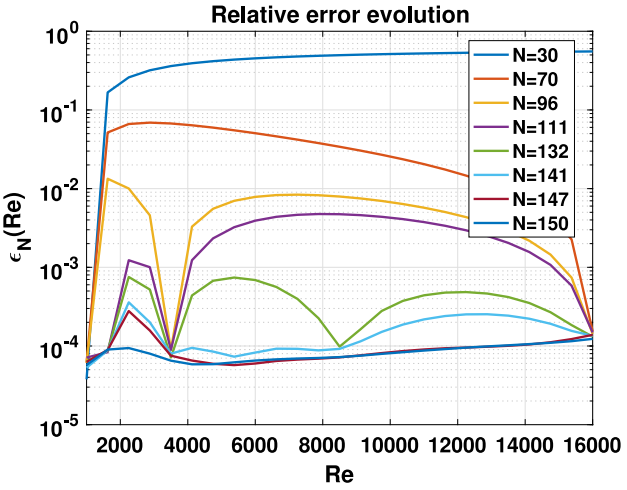

Fig. 7. Error $\epsilon_N(\mu)$ in each iteration of the POD+Greedy algorithm, using the exact error as error indicator.

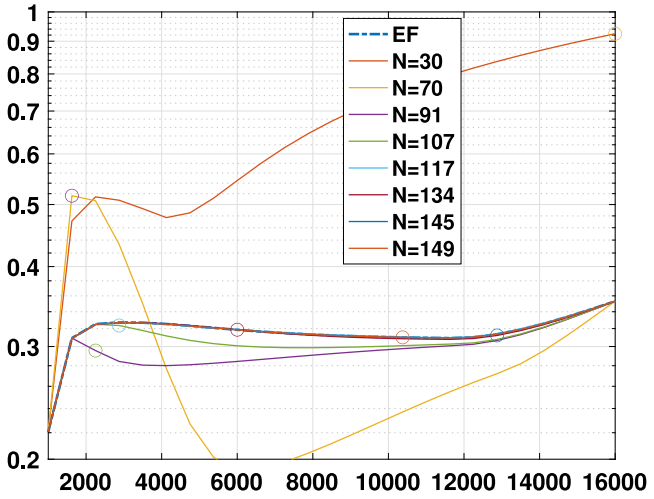

Fig. 8. Evolution of the ROM estimator, $\Delta_N(\mu)$, in each iteration of the Greedy algorithm, versus the FOM estimator, $\Delta_h(\mu)$. For each iteration, we plot the error indicator for every parameter in the range, and we highlight with a circle the parameter selected for the next iteration.

Table 3
Validation of RB model.

μ	3000	6000	9000	12 000	15 000
T_{FE}	59.11 s	59.05 s	58.80 s	58.82 s	59.48 s
T_{RB}	3.28 s	3.29 s	3.26 s	3.23 s	3.23 s
Speed-up	18.02	17.95	18.04	18.21	18.41
$\Delta_N(\mu)$	0.327244	0.318597	0.311507	0.309537	0.337665
$\Delta_h(\mu)$	0.326930	0.318601	0.311539	0.309520	0.337642
$\epsilon_N(\mu)$	$7.93 \cdot 10^{-5}$	$6.05 \cdot 10^{-5}$	$7.70 \cdot 10^{-5}$	$8.37 \cdot 10^{-5}$	$10.83 \cdot 10^{-5}$

is shown in Fig. 8. In Table 3, we show for several values of the parameter, which do not correspond to those chosen by the Greedy algorithm, the calculation times of the finite element method T_{FE} and of the reduced method T_{RB} as well as the corresponding speed-up. The lower part shows the values corresponding to the indicators $\Delta_N(\mu)$, $\Delta_h(\mu)$ and the exact error $\epsilon_N(\mu)$ committed for the different cases. All data have been obtained from the eight iteration with $N = 149$. The speed-up obtained is close to 18 in each of the cases tested. The values of the indicators $\Delta_N(\mu)$, $\Delta_h(\mu)$, except in one case, have three coincident decimal places.

We can conclude that the error indicator has been successfully extended from parametric linear parabolic problems to LES parametric turbulence models, obtaining relative errors in the order of 10^{-4}. In Fig. 9, we show the comparison between the FE (left) and RB (centre) velocity field, with the absolute error (right) between them, for a Reynolds value $\mu = 15\,000$, and times

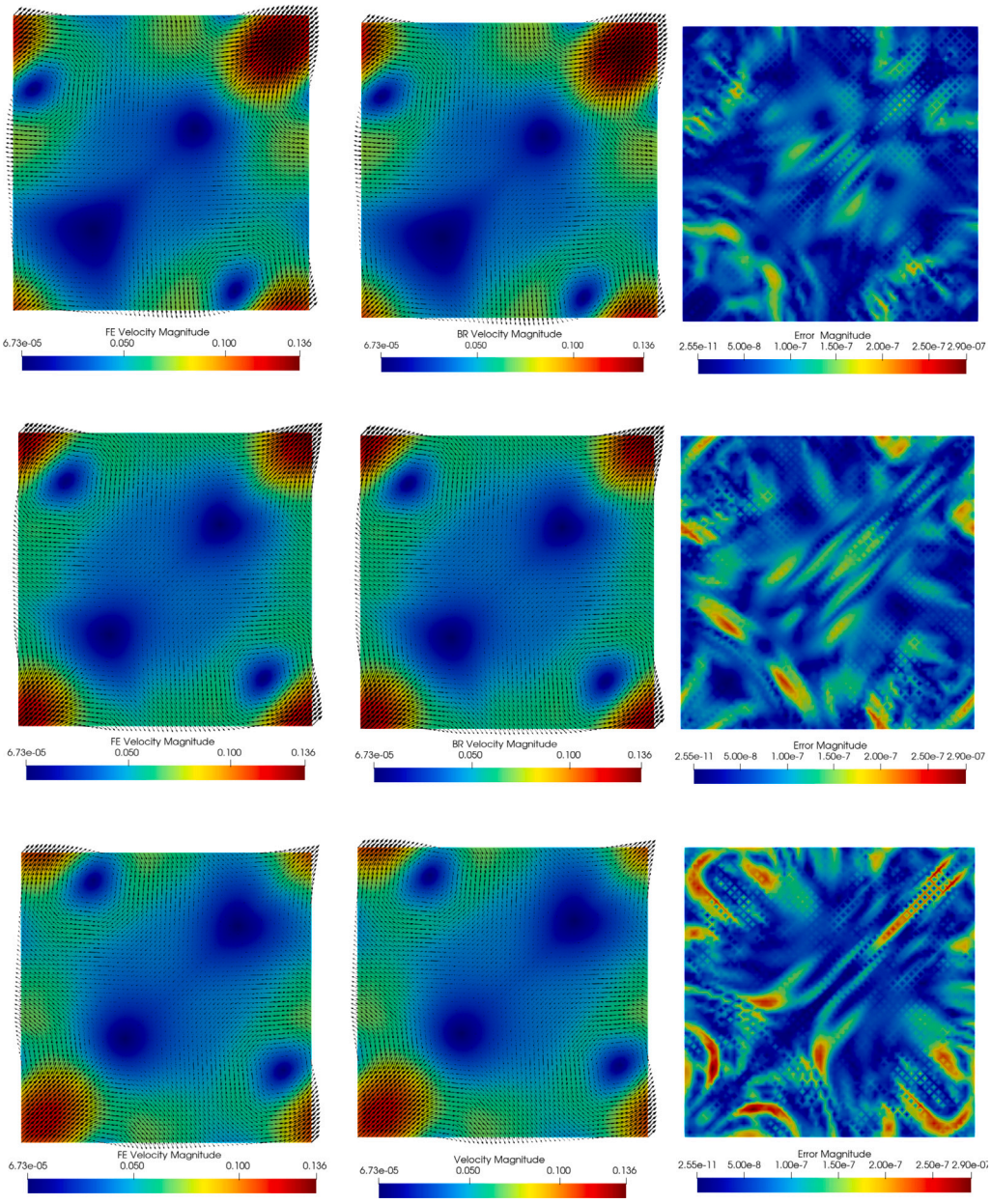

Fig. 9. Comparison between FE (left) and RB (centre) velocity field, and the absolute error (right), for $\mu = 15\,000$, at $T = 20\text{ s}, 25\text{ s}, 30\text{ s}$ from top to bottom.

$T = 20, 25, 30$ s (from top to bottom), where we can observe that the difference between both FE and RB velocity field is practically negligible, since the maximum of the absolute error between both fields is less that 10^{-7}. Moreover, in Fig. 10 we show the temporal evolution of the velocity magnitude for some spatial locations, in (0, 0), (0.25, 0.25) and (0.5, 0.5) for both the high FE solution and the RB solution for a Reynolds parameter value of $\mu = 15\,000$. We can observe the regularity of the flow for both the FE and RB solution.

5.6. Equispaced sampling

The objective of this second test is to compare the results obtained in the previous test with the ones obtained when considering equispaced parameter values, instead of considering a Greedy algorithm for selecting them.

In Table 4, we present the maximum relative error and the l_2-norm of the relative error in the parameter range. We also present in Fig. 11 the evolution of the relative error in the range of the parameter, we can see that the largest errors appear in the lower Reynolds number range, at which the decrease is slower as N increases.

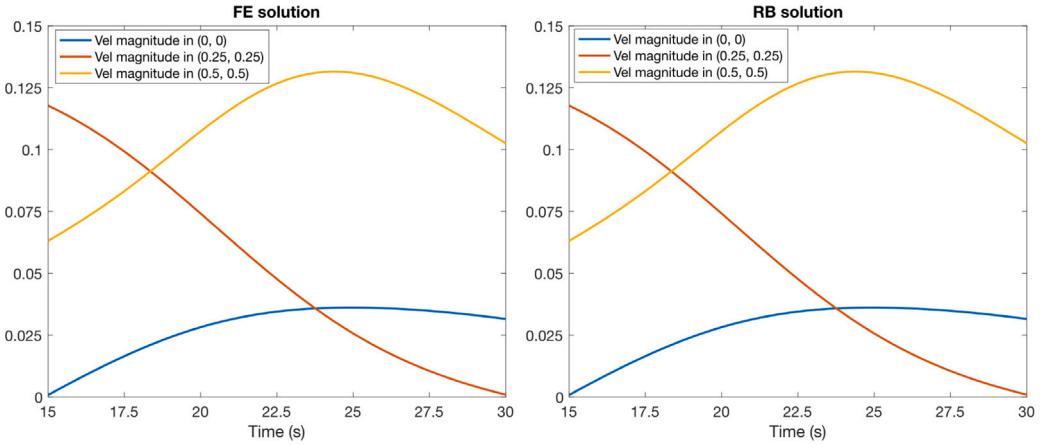

Fig. 10. Temporal evolution of the velocity magnitude at $\mathbf{x} = (0, 0)$, $\mathbf{x} = (0.25, 0.25)$ and $\mathbf{x} = (0.5, 0.5)$. Left panel: FE solution. Right panel: RB solution.

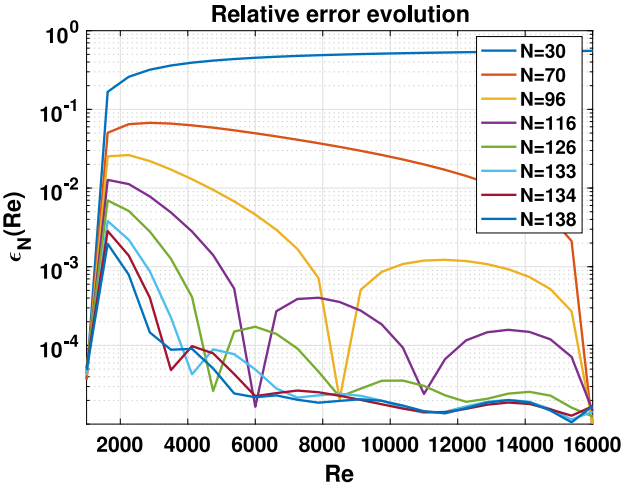

Fig. 11. Convergence story of POD+Greedy, using equispaced parameter values.

Table 4
Convergence of the POD+Greedy algorithm, using equispaced parameter values.

It.	N	$\max_{Re}\epsilon_N(Re)$	$l_2(\epsilon_N(Re))$
1	30	$3,65 \cdot 10^{-1}$	$5,53 \cdot 10^{-1}$
2	70	$6,74 \cdot 10^{-2}$	$1,95 \cdot 10^{-1}$
3	96	$2,63 \cdot 10^{-2}$	$4,95 \cdot 10^{-2}$
4	116	$1,27 \cdot 10^{-2}$	$1,96 \cdot 10^{-2}$
5	126	$6,96 \cdot 10^{-3}$	$9,18 \cdot 10^{-3}$
6	133	$3,81 \cdot 10^{-3}$	$4,49 \cdot 10^{-3}$
7	134	$2,85 \cdot 10^{-3}$	$3,20 \cdot 10^{-3}$
8	138	$1,96 \cdot 10^{-3}$	$2,12 \cdot 10^{-3}$

Finally, we compare all the presented procedures in Fig. 12. We present, in Fig. 12(a), the comparison of the decay of the l_2-norm of the relative error over the parameter range and, in Fig. 12(b) the comparison of the decay of the maximum relative error over the parameter range. We observe a spectral convergence with respect to the dimension of the reduced space N. We also observe that the *a posteriori* error indicator based on Kolmogorov's law and the Complete POD procedure presented in Section 5.2, provides very similar results compared to the ones obtained using the exact error, in both l_2 and maximum relative error decay. Also, we observe that it provides better results than just selecting equispaced parameters in the reduced basis construction, specially in the maximum relative error. This is due to the fact that for equispaced sampling the errors are localized in the lower Reynolds numbers, whereas thanks to our approach the information about these parameters are included in the construction of the reduced basis, therefore reducing the maximum error. Let us recall that the simple equispaced polynomial interpolation may present exponential decay if

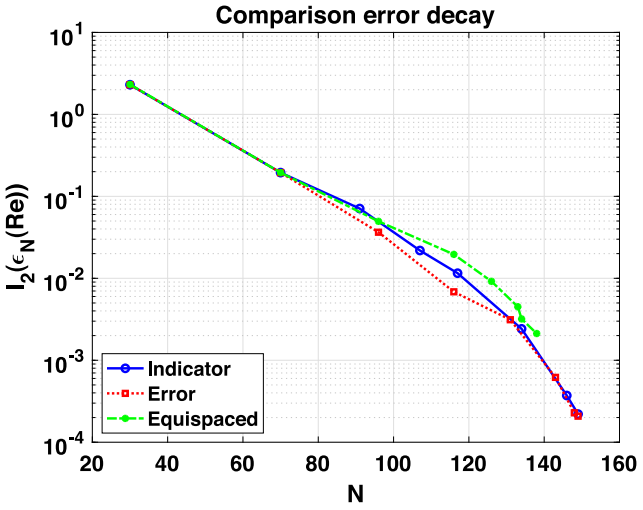

(a) Comparison of relative l_2-norm decay.

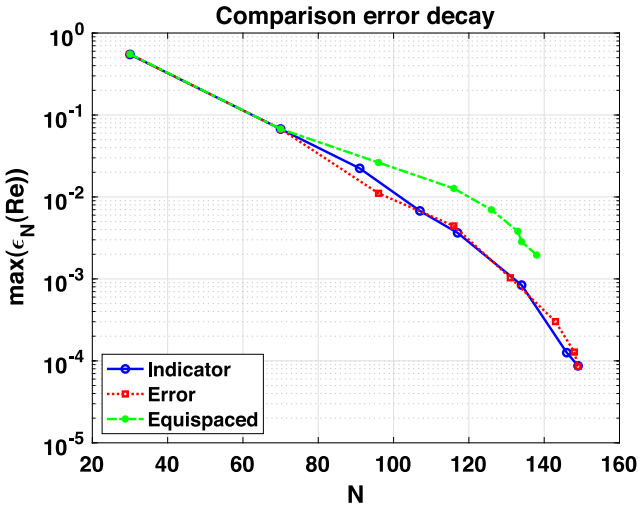

(b) Comparison of relative l_∞-norm decay.

Fig. 12. Comparison of the relative error decay for the different methods. In both panels, the errors obtained by means of the a posteriori error indicator appear in continuous blue fashion with circles, the errors obtained using the real error appear in dashed red fashion with squares and the errors obtained using equispaced parameters are shown in dash-dotted green fashion with asterisks.

there is an analytic dependence with respect to the parameter in a domain large enough. This fact possibly plays a role here, as the flow is quite smoothly changing as the Reynolds number changes.

6. Conclusions

In this work, we introduce a Reduced Basis model for turbulence at statistical equilibrium. This is based upon an a-posteriori error estimation procedure that measures the distance from a trial solution to the theoretical $k^{-5/3}$ energy spectrum. Upon this error estimation procedure, we have used a Greedy Algorithm to build the reduced basis for the Smagorinsky turbulence model. We have adapted the error estimation to stagnation situations in the Greedy Algorithm, by comparing the energy spectrum of the trial solution with that of the current RB solution, as a surrogate of the FOM solution. We have also carried on an error analysis that clarifies the role of the energy-spectrum error estimator, as the FOM–ROM error is driven by this estimator, plus the projection error on the reduced space.

The RB Smagorinsky model has been tested for some academic, yet meaningful, 2D flows, as these present the Kolmogorov's K41 Theory energy spectrum profile. In these tests the Reynolds number acts as a parameter. We have obtained error levels quite close to those provided by the optimal RB Smagorinsky model obtained if we replace the error estimator by the exact ROM–FOM error in the Greedy Algorithm. Both errors present a similar exponential decay as the dimension of the reduced spaces increases, in

both L^2 and L^∞ parametric norms. We have also tested the new RB method versus the RB Smagorinsky method constructed with equally-spaced snapshots, that present a much slower decay in L^∞ parametric norm.

In addition, we obtain speed-up ratios of computational time close to 20.

The interest of this novel a posteriori error indicator is that it applies to any kind of parameter (either geometrical or physical) and to any kind of numerical discretization. The only requirement is that the targeted flows have a well developed inertial spectrum, and that the numerical solver is able to reproduce a part of this inertial spectrum, what is well achieved by current solvers.

At present we work to apply the overall procedure to 3D flows, as well as to some kinds of non-equilibrium flows, for which the energy spectrum still obeys specific laws (cf. [45]).

CRediT authorship contribution statement

Alejandro Bandera Moreno: Software, Supervision, Writing – origin draft, Writing – review & editing. **Cristina Caravaca García:** Software, Writing – origin draft. **Tomás Chacón Rebollo:** Conceptualization, Supervision, Writing – origin draft, Writing – review & editing. **Enrique Delgado Ávila:** Software, Supervision, Writing – origin draft, Writing – review & editing. **Macarena Gómez Mármol:** Conceptualization, Supervision, Writing – origin draft, Writing – review & editing.

Declaration of competing interest

The authors declare that they have no known competing financial interests or personal relationships that could have appeared to influence the work reported in this paper.

Data availability

No data was used for the research described in the article.

Acknowledgements

This work has been funded by the Spanish Government Project PID2021-123153OB-C21 and European Union's Horizon 2020 research and innovation programme under the Marie Sklodowska–Curie Actions, grant agreement 872442 (ARIA).

Appendix. Proof of some results

A.1. Proof of Proposition 1

Let be $\mathbf{u}_1$ and $\mathbf{u}_2$ are the velocity fields of two locally isotropic flows, and taking into account Eqs. , then we obtain the following upper bound

$$|\nu_T(\mathbf{u}_1) - \nu_T(\mathbf{u}_2)| \leq$$
$$\leq C\,h^2 \left| \left(\int_{k_1}^{k_c} k^2 E(k)(k;\mathbf{u}_1) dk \right)^{1/2} - \left(\int_{k_1}^{k_c} k^2 E(k)(k;\mathbf{u}_2)|\, dk \right)^{1/2} \right|,$$

Now, noting that $\int_{k_1}^{k_c} k^2 E(k)(k;\mathbf{u}_i) dk \geq 0,\ i = 1,2$, we have

$$|\nu_T(\mathbf{u}_1) - \nu_T(\mathbf{u}_2)| \leq C\,h^2 \left| \int_{k_1}^{k_c} k^2 \left(E(k)(k;\mathbf{u}_1) - E(k)(k;\mathbf{u}_2) \right) dk \right|^{1/2}.$$

This yields the first result of the proposition, estimate (17).

For estimate (18), as $|E(k)(k;\mathbf{u}_1) - E(k)(k;\mathbf{u}_2)| \leq \delta, \forall k \in [k_1, k_c]$, then the integral becomes

$$\int_{k_1}^{k_c} k^2\, |E(k)(k;\mathbf{u}_1) - E(k)(k;\mathbf{u}_2)|\, dk$$
$$\leq \delta \int_{k_1}^{k_c} k^2 dk = \frac{1}{3}\delta(k_c^3 - k_1^3) \leq \frac{1}{3}\delta k_c^3 \approx \frac{1}{3}\delta h^{-3},$$

where we have used that $k_1 \geq 0$, and that $k_c \approx h^{-1}$. Including this result in the previous equation, we obtain

$$|\nu_T(\mathbf{u}_1) - \nu_T(\mathbf{u}_2)| \leq C\,h^2(\delta h^{-3})^{1/2} \leq C(h\delta)^{1/2},$$

and that is the desired result.

A.2. Sketch of the proof of Theorem 2

We consider the weak formulation arising from Eq. (3) for $\mathbf{u}_1$, $\mathbf{u}_2$ and the same test function $\mathbf{v}$ belonging to $W^{1,3}(\Omega)$. If we subtract one from the other, and denoting $\nu = 1/\mu$, $\boldsymbol{e} = \mathbf{u}_1 - \mathbf{u}_2$, we get to

$$\begin{aligned}(\frac{\partial}{\partial t}\boldsymbol{e}, \mathbf{v})_\Omega + a(\boldsymbol{e}, \mathbf{v}; \mu) + c(\mathbf{u}_1, \mathbf{u}_1, \mathbf{v}; \mu) - c(\mathbf{u}_2, \mathbf{u}_2, \mathbf{v}; \mu) \\ + a_S(\mathbf{u}_1; \mathbf{u}_1, \mathbf{v}; \mu) - a_S(\mathbf{u}_2; \mathbf{u}_2, \mathbf{v}; \mu) = 0, \ \forall \mathbf{v}.\end{aligned} \tag{A.1}$$

If we consider $\mathbf{v} = \boldsymbol{e}$, then we have the following identities

- $(\frac{\partial}{\partial t}\boldsymbol{e}, \boldsymbol{e})_\Omega + a(\boldsymbol{e}, \boldsymbol{e}; \mu) = \frac{1}{2}\frac{\partial}{\partial t}\|\boldsymbol{e}\|_2^2 + \nu\|\nabla \boldsymbol{e}\|_2^2$,
- $c(\mathbf{u}_1, \mathbf{u}_1, \boldsymbol{e}; \mu) - c(\mathbf{u}_2, \mathbf{u}_2, \boldsymbol{e}; \mu) \pm c(\mathbf{u}_2, \mathbf{u}_1, \boldsymbol{e}; \mu) = c(\boldsymbol{e}, \mathbf{u}_1, \boldsymbol{e}; \mu) - c(\mathbf{u}_2, \boldsymbol{e}, \boldsymbol{e}; \mu) = c(\boldsymbol{e}, \mathbf{u}_1, \boldsymbol{e}; \mu)$,
- $a_S(\mathbf{u}_1; \mathbf{u}_1, \boldsymbol{e}; \mu) - a_S(\mathbf{u}_2; \mathbf{u}_2, \boldsymbol{e}; \mu) \pm a_S(\mathbf{u}_1; \mathbf{u}_2, \boldsymbol{e}; \mu) = a_S(\mathbf{u}_1; \boldsymbol{e}, \boldsymbol{e}; \mu) + (a_S(\mathbf{u}_1; \mathbf{u}_2, \boldsymbol{e}; \mu) - a_S(\mathbf{u}_2; \mathbf{u}_2, \boldsymbol{e}; \mu))$.

Introducing them in the previous equation and rearranging the terms, we have

$$\begin{aligned}\frac{1}{2}\frac{\partial}{\partial t}\|\boldsymbol{e}\|_2^2 + \nu\|\nabla \boldsymbol{e}\|_2^2 + a_S(\mathbf{u}_1; \boldsymbol{e}, \boldsymbol{e}; \mu) = \\ = -c(\boldsymbol{e}, \mathbf{u}_1, \boldsymbol{e}; \mu) - (a_S(\mathbf{u}_1; \mathbf{u}_2, \boldsymbol{e}; \mu) - a_S(\mathbf{u}_2; \mathbf{u}_2, \boldsymbol{e}; \mu)).\end{aligned} \tag{A.2}$$

The second and third terms can be bounded by the minimum effective viscosity as $\nu\|\nabla \boldsymbol{e}\|_2^2 + a_S(\mathbf{u}_1; \boldsymbol{e}, \boldsymbol{e}; \mu) \geq \nu_e\|\nabla \boldsymbol{e}\|_2^2$, with

$$\nu_e = \nu + (C_S\, h)^2 \ \max\left\{ \inf_{\Omega\times[0,T]} |\nabla \mathbf{u}_1|, \inf_{\Omega\times[0,T]} |\nabla \mathbf{u}_2| \right\}.$$

After taking absolute value in both terms, thanks to the regularity of $\mathbf{u}_1$ and $\mathbf{u}_2$, we can bound each term on the right-hand side as in the following:

$$\begin{aligned}|c(\boldsymbol{e}, \mathbf{u}_1, \boldsymbol{e}; \mu)| &\leq C\|\boldsymbol{e}\|_2\|\nabla \mathbf{u}_1\|_3\|\boldsymbol{e}\|_6 + C\|\boldsymbol{e}\|_2\|\nabla \boldsymbol{e}\|_2\|\mathbf{u}_1\|_\infty \\ &\leq \frac{C\epsilon}{2}\|\nabla \boldsymbol{e}\|_2^2 + \frac{C(\mathbf{u}_1)}{2\epsilon}\|\boldsymbol{e}\|_2^2,\end{aligned} \tag{A.3}$$

where we have followed the same estimate procedure as in [20, Chapter 9], and we have used Sobolev's embeddings, Cauchy–Bunyakovsky–Schwarz (CBS) and Hölder's inequalities. For the second term, we obtain:

$$(a_S(\mathbf{u}_1; \mathbf{u}_2, \boldsymbol{e}; \mu) - a_S(\mathbf{u}_2; \mathbf{u}_2, \boldsymbol{e}; \mu)) \leq \frac{C(\mathbf{u}_2)}{2\epsilon}|\nu_T(\mathbf{u}_1) - \nu_T(\mathbf{u}_2)|^2 + \frac{C\epsilon}{2}\|\nabla \boldsymbol{e}\|_2^2,$$

where we have made use of CBS and Hölder's inequality. Taking into account the dependence on $\mathbf{u}_1$, $\mathbf{u}_2$ of the constants, their role can be exchanged if we modify how we obtain the corresponding terms.

Taking all of the above into account, we arrive at

$$\frac{1}{2}\frac{\partial}{\partial t}\|\boldsymbol{e}\|_2^2 + (\nu_e - C\epsilon)\|\nabla \boldsymbol{e}\|_2^2 \leq \frac{C}{2\epsilon}\|\boldsymbol{e}\|_2^2 + \frac{C}{2\epsilon}|\nu_T(\mathbf{u}_1) - \nu_T(\mathbf{u}_2)|^2.$$

Now, we can select $\epsilon = \nu_e/(2C)$ and multiply both terms by 2 to obtain

$$\frac{\partial}{\partial t}\|\boldsymbol{e}\|_2^2 + \nu_e\|\nabla \boldsymbol{e}\|_2^2 \leq \frac{C}{\nu_e}\|\boldsymbol{e}\|_2^2 + \frac{C}{\nu_e}|\nu_T(\mathbf{u}_1) - \nu_T(\mathbf{u}_2)|^2 \leq \frac{C}{\nu_e}\|\boldsymbol{e}\|_2^2 + \frac{C}{\nu_e}\delta h,$$

where we have also used Proposition 1 in the last inequality.

Finally, using Grönwall's lemma, in the standard way, we obtain the desired result.

A.3. Sketch of the proof of Theorem 3

Let $\mathbf{u}_h$ be the solution of the FOM Smagorinsky model (6) and $\mathbf{u}_N$ the solution of ROM Smagorinsky model (10). Also, we denote by $\boldsymbol{w}_N$ the projection of $\mathbf{u}_h$ into the reduced space, and $\boldsymbol{\rho}_N = \boldsymbol{w}_N - \mathbf{u}_h$. For the sake of clarity, we will denote by ∂_t the time derivative.

We start from Eq. (6), taking $q_h = p_h$, we add and subtract $(\partial_t \boldsymbol{w}_N, \mathbf{v}_h) + \nu(\nabla \boldsymbol{w}_N, \nabla \mathbf{v}_h)$, and we obtain the following

$$\begin{aligned}(\partial_t \boldsymbol{w}_N, \mathbf{v}_h)_\Omega + a(\boldsymbol{w}_N, \mathbf{v}_h; \mu) + a_S(\mathbf{u}_h; \mathbf{u}_h, \mathbf{v}_h; \mu) + c(\mathbf{u}_h, \mathbf{u}_h, \mathbf{v}_h; \mu) \\ = \langle \mathbf{f}, \mathbf{v}_h\rangle + (\partial_t \boldsymbol{\rho}_N, \mathbf{v}_h)_\Omega + a(\boldsymbol{\rho}_N, \mathbf{v}_h; \mu), \quad \forall \mathbf{v}_h \in Y_h.\end{aligned}$$

Now, we consider $\mathbf{v}_h = \mathbf{v}_N \in Y_N$, and we subtract Eq. (10) by considering $q_N = p_N$. If we name $\boldsymbol{e}_N = \boldsymbol{w}_N - \mathbf{u}_N$, then, we obtain

$$\begin{aligned}(\partial_t \boldsymbol{e}_N, \mathbf{v}_N)_\Omega + a(\boldsymbol{e}_N, \mathbf{v}_N; \mu) + (a_S(\mathbf{u}_h; \mathbf{u}_h, \mathbf{v}_N; \mu) - a_S(\mathbf{u}_N; \mathbf{u}_N, \mathbf{v}_N; \mu)) \\ + (c(\mathbf{u}_h, \mathbf{u}_h, \mathbf{v}_N; \mu) - c(\mathbf{u}_N, \mathbf{u}_N, \mathbf{v}_N; \mu)) = (\partial_t \boldsymbol{\rho}_N, \mathbf{v}_N)_\Omega + a(\boldsymbol{\rho}_N, \mathbf{v}_N; \mu).\end{aligned}$$

Considering $\mathbf{v}_N = \boldsymbol{e}_N$ and $\nu = 1/\mu$, and making the same kind of manipulations as in the proof of Theorem 2, we get to

$$\begin{aligned}\frac{1}{2}\partial_t\|\boldsymbol{e}_N\|^2 + \nu\|\nabla \boldsymbol{e}_N\|_2^2 + a_S(\mathbf{u}_h; \boldsymbol{e}_N, \boldsymbol{e}_N; \mu) \\ = (\partial_t \boldsymbol{\rho}_N, \boldsymbol{e}_N)_\Omega + a(\boldsymbol{\rho}_N, \boldsymbol{e}_N; \mu) + a_S(\mathbf{u}_h; \boldsymbol{\rho}_N, \boldsymbol{e}_N; \mu) \\ + c(\mathbf{u}_h, \boldsymbol{\rho}_N, \boldsymbol{e}_N; \mu) + c(\boldsymbol{\rho}_N, \boldsymbol{w}_N, \boldsymbol{e}_N; \mu) - c(\boldsymbol{e}_N, \boldsymbol{w}_N, \boldsymbol{e}_N; \mu). \\ + (a_S(\mathbf{u}_h; \mathbf{u}_h, \boldsymbol{e}_N; \mu) - a_S(\mathbf{u}_N; \mathbf{u}_h, \boldsymbol{e}_N; \mu)).\end{aligned}$$

As we did in the previous proof, we can define the effective minimum viscosity ν_e to bound the last two terms in the left-hand side. For the right-hand side, we obtain the following bounds

$$
\begin{aligned}
&|(\partial_t \boldsymbol{\rho}_N, \boldsymbol{e}_N)_\Omega + a(\boldsymbol{\rho}_N, \boldsymbol{e}_N; \mu) + a_S(\mathbf{u}_h; \boldsymbol{\rho}_N, \boldsymbol{e}_N; \mu)| \\
&\quad \leq C\|\partial_t \boldsymbol{\rho}_N\|_2^2 + C\|\boldsymbol{e}_N\|_2^2 + \frac{\nu}{2\epsilon_*}\|\nabla \boldsymbol{\rho}_N\|_2^2 + \frac{\nu\epsilon_*}{2}\|\nabla \boldsymbol{e}_N\|_2^2 \\
&\qquad + \frac{C}{2\epsilon}\|\nu_T(\mathbf{u}_h)\nabla \boldsymbol{\rho}_N\|_2^2 + \frac{C\epsilon}{2}\|\nabla \boldsymbol{e}_N\|_2^2. \\
&|c(\mathbf{u}_h, \boldsymbol{\rho}_N, \boldsymbol{e}_N; \mu) + c(\boldsymbol{\rho}_N, \boldsymbol{w}_N, \boldsymbol{e}_N; \mu) - c(\boldsymbol{e}_N, \boldsymbol{w}_N, \boldsymbol{e}_N; \mu)| \\
&\quad \leq \frac{C}{2\epsilon}\|\nabla \mathbf{u}_h\|_2^2\|\nabla \boldsymbol{\rho}_N\|_2^2 + \frac{C\epsilon}{2}\|\nabla \boldsymbol{e}_N\|_2^2 \\
&\qquad + \frac{C}{2\epsilon}\|\nabla \boldsymbol{w}_N\|_2^2\|\nabla \boldsymbol{\rho}_N\|_2^2 + \frac{C\epsilon}{2}\|\nabla \boldsymbol{e}_N\|_2^2 \\
&\qquad + \frac{C}{2\epsilon}\left(\|\nabla \boldsymbol{w}_N\|_3^2 + \|\boldsymbol{w}_N\|_\infty^2\right)\|\boldsymbol{e}_N\|_2^2 + \frac{C\epsilon}{2}\|\nabla \boldsymbol{e}_N\|_2^2,
\end{aligned}
$$

where the last term is bounded by (A.3).

$$
\begin{aligned}
&|(a_S(\mathbf{u}_h; \mathbf{u}_h, \boldsymbol{e}_N; \mu) - a_S(\mathbf{u}_N; \mathbf{u}_h, \boldsymbol{e}_N; \mu))| \\
&\quad \leq \frac{C}{2\epsilon}\|\nu_T(\mathbf{u}_h) - \nu_T(\mathbf{u}_N)\|_\infty^2\|\nabla \mathbf{u}_h\|_2^2 + \frac{C\epsilon}{2}\|\nabla \boldsymbol{e}_N\|_2^2.
\end{aligned}
$$

For obtaining the previous bounds, we have used extensively CBS and Hölder's inequalities.

Arranging the terms, and selecting the suitable ϵ and ϵ_*, we get to the following result

$$
\begin{aligned}
&\partial_t\|\boldsymbol{e}_N\|^2 + \nu_e\|\nabla \boldsymbol{e}_N\|_2^2 \\
&\quad \leq C\|\partial_t \boldsymbol{\rho}_N\|_2^2 + \frac{C}{\nu_e}\left(\nu + \|\nabla \mathbf{u}_h\|_2^2 + \|\nabla \boldsymbol{w}_N\|_2^2\right)\|\nabla \boldsymbol{\rho}_N\|_2^2 + \frac{C}{\nu_e}\|\nu_T(\mathbf{u}_h)\nabla \boldsymbol{\rho}_N\|_2^2 \\
&\qquad + C\left(1 + \frac{\|\nabla \boldsymbol{w}_N\|_3^2 + \|\boldsymbol{w}_N\|_\infty^2}{\nu_e}\right)\|\boldsymbol{e}_N\|_2^2 + \frac{C}{\nu_e}\|\nu_T(\mathbf{u}_h) - \nu_T(\mathbf{u}_N)\|_\infty^2\|\nabla \mathbf{u}_h\|_2^2.
\end{aligned}
$$

Now, using Proposition 1, and applying Grönwall's inequality, we get to estimate (20).

References

[1] J.S. Hesthaven, G. Rozza, B. Stamm, Certified Reduced Basis Methods for Parametrized Partial Differential Equations, Springer, 2015.
[2] P. Holmes, G. Berkooz, Coherent Structures, Dynamical Systems and Symmetry, Cambridge, 1996.
[3] A. Quarteroni, A. Manzoni, F. Negri, Reduced Basis Methods for Partial Differential Equations: An Introduction, Springer, 2015.
[4] K. Kunisch, S. Volkwein, Galerkin proper orthogonal decomposition methods for a general equation in fluid dynamics, SIAM J. Numer. Anal. 40 (2002) 492–515.
[5] R. Pinnau, Model reduction via proper orthogonal decomposition, in: W. Schilders, H. van der Vorst, J. Rommes (Eds.), Mathematics in Industry, Springer, Berlin, Heidelberg, 2008, pp. 95–109.
[6] S. Busto, G. Stabile, G. Rozza, M.E. Vázquez-Cendón, Pod–Galerkin reduced order methods for combined navier–stokes transport equations based on a hybrid FV-FE solver, Comput. Math. Appl. 79 (2020) 256–273.
[7] M. Couplet, P. Sagaut, C. Basdevant, Intermodal energy transfers in a proper orthogonal decomposition-galerkin representation of a turbulent separated flow, J. Fluid Mech. 491 (2003) 275–284.
[8] S. Hijazi, M. Freitag, N. Landwehr, Pod-galerkin reduced order models and physics-informed neural networks for solving inverse problems for the Navier–Stokes equations, Adv. Model. Simul. Eng. Sci. 10 (2023) 1–38.
[9] F. Negri, A. Manzoni, G. Rozza, Reduced basis approximation of parametrized optimal flow control problems for the Stokes equations, Comput. Math. Appl. 69 (2015) 319–336.
[10] G. Stabile, G. Rozza, Finite volume POD-galerkin stabilised reduced order methods for the parametrised incompressible Navier-Stokes equations, Comput. & Fluids 173 (2018) 273–284.
[11] M.A. Grepl, Y. Maday, N.C. Nguyen, A.T. Patera, Efficient reduced-basis treatment of nonaffine and nonlinear partial differential equations, ESAIM Math. Model. Numer. Anal. 41 (2007) 575–605.
[12] S. Ali, F. Ballarin, G. Rozza, Stabilized reduced basis methods for parametrized steady Stokes and Navier-Stokes equations, Comput. Math. Appl. 80 (2020) 2399–2416.
[13] F. Ballarin, A. Manzoni, A. Quarteroni, G. Rozza, Supremizer stabilization of POD-Galerkin approximation of parametrized steady incompressible Navier-Stokes equations, Int. J. Numer. Methods Eng. 102 (2014) 1136–1161.
[14] S. Deparis, Reduced basis error bound computation of parameter-dependent Navier-Stokes equations by the natural norm approach, SIAM J. Sci. Comput. 46 (2008) 2039–2067.
[15] S. Deparis, G. Rozza, Reduced basis method for multi-parameter-dependent steady Navier-Stokes equations: Applications to natural convection in a cavity, J. Comput. Phys. 228 (2009) 4359–4378.
[16] A. Manzoni, An efficient computational framework for reduced basis approximation and a posteriori error estimation of parametrized Navier-Stokes flows, ESAIM Math. Model. Numer. Anal. 48 (2014) 1199–1226.
[17] L. Fick, Y. Maday, A.T. Patera, T. Taddei, A stabilized pod model for turbulent flows over a range of reynolds numbers: Optimal parameter sampling and constrained projection, J. Comput. Phys. 371 (2018) 214–243.
[18] P.-H. Tsai, P. Fischer, Parametric model-order-reduction development for unsteady convection, Front. Phys. 10 (2022).
[19] F. Bouchon, T. Dubois, F. Jauberteau, Dynamic multilevel methods and non-homogeneous turbulence, in: Sixteenth International Conference on Numerical Methods in Fluid Dynamics: Proceedings of the Conference Held in Arcachon, France, 6–10 1998, Springer, 1998, pp. 123–128.
[20] T. Chacón Rebollo, R. Lewandowski, Mathematical and Numerical Foundations of Turbulence Models and Applications, Springer, New York, 2014.
[21] A.N. Kolmogorov, The local structure of turbulence in incompressible viscous fluid for very large reynolds number, Dokl. Akad. Nauk. SSSR 30 (1941) 301–303.

[22] L. Onsager, Statistical hydrodynamics, Il Nuovo Cimento (1943-1954) 6 (1949) 279–287.
[23] L.F. Richardson, Weather Prediction by Numerical Process, University Press, 1922.
[24] S. Hijazi, S. Ali, G. Stabile, F. Ballarin, G. Rozza, The effort of increasing reynolds number in projection-based reduced order methods: from laminar to turbulent flows, in: Numerical Methods for Flows: FEF 2017 Selected Contributions, 2020, pp. 245–264.
[25] S. Hijazi, G. Stabile, A. Mola, G. Rozza, Data-driven Pod-Galerkin reduced order model for turbulent flows, J. Comput. Phys. 416 (2020) 109513.
[26] Z. Wang, I. Akhtar, J. Broggaard, T. Iliescu, Proper orthogonal decomposition closure models for turbulent flows: A numerical comparison, Comp. Meth. Appl Mech. Engrg. 237-240 (2012) 10–26.
[27] Z. Wang, T. Iliescu, Variational multiscale proper orthogonal decomposition: Navier-Stokes equations, Num. Meth. PDEs 30 (2014) 641–663.
[28] M. Girfoglio, A. Quaini, G. Rozza, A linear filter regularization for POD-based reduced-order models of the quasi-geostrophic equations, C. R. Méc. 351 (2023) 1–21.
[29] M. Girfoglio, A. Quaini, G. Rozza, A novel large eddy simulation model for the quasi-geostrophic equations in a finite volume setting, J. Comput. Appl. Math. 418 (2023) 114656.
[30] S.E. Ahmed, S. Pawar, O. San, A. Rasheed, T. Iliescu, B.R. Noack, On closures for reduced order models—a spectrum of first-principle to machine-learned avenues, Phys. Fluids 33 (2021).
[31] S.E. Ahmed, O. San, A. Rasheed, T. Iliescu, A. Veneziani, Physics guided machine learning for variational multiscale reduced order modeling, SIAM J. Sci. Comput. 45 (2023) B283–B313.
[32] W. Snyder, C. Mou, H. Liu, O. San, R. DeVita, T. Iliescu, Reduced order model closures: a brief tutorial, in: Recent Advances in Mechanics and Fluid-Structure Interaction with Applications, Springer International Publishing, 2022, pp. 167–193.
[33] F. Ballarin, T. Chacón Rebollo, E. Delgado Ávila, M. Gómez Mármol, G. Rozza, Certified reduced basis VMS-smagorinsky model for natural convection flow in a cavity with variable height, Comput. Math. Appl. 80 (2020) 973–989.
[34] C. Caravaca García, Reduced Basis Method applied to the Smagorinsky Turbulence Model (Ph.D. thesis), Universidad de Sevilla, 2022.
[35] T. Chacón Rebollo, E. Delgado Ávila, M. Gómez Mármol, On a certified VMS-Smagorinsky reduced basis model with LPS pressure stabilisation, Appl. Numer. Math. 185 (2023) 365–385.
[36] T. Chacón Rebollo, E. Delgado Ávila, M. Gómez Mármol, F. Ballarin, G. Rozza, On a certified Smagorinsky reduced basis turbulence model, SIAM J. Numer. Anal. 55 (2017) 3047–3067.
[37] F. Brezzi, J. Rappaz, P. Raviart, Finite dimensional approximation of nonlinear problems, Numer. Maht. 36 (1980) 1–25.
[38] M. Barrault, Y. Maday, N.C. Nguyen, A.T. Patera, An 'empirical interpolation' method: application to efficient reduced-basis discretization of partial differential equations, C.R. Acad. Sci. Paris Sér. I Math. 339 (2004) 667–672.
[39] Y. Maday, N.C. Nguyen, A.T. Patera, G.S.H. Pau, A general, multipurpose interpolation procedure: the magic points, Commun. Pure Appl. Anal. 8 (2009) 383–404.
[40] B. Haasdonk, Convergence rates of the POD-greedy method, ESAIM Math. Model. Numer. Anal. 47 (2013) 859–873.
[41] P.G. Ciarlet, The Finite Element Method for Elliptic Problems, North-Holland, Amsterdam, 1978.
[42] R.H. Kraichnan, Inertial ranges in two-dimensional turbulence, Phys. Fluids 10 (1967) 1417–1423.
[43] B. Haasdonk, Reduced basis methods for parametrized pdes–a tutorial introduction for stationary and instationary problems, Model Reduct. Approx. Theory Algorithms 15 (2017) 65.
[44] C. Himpe, T. Leibner, S. Rave, Hierarchical approximate proper orthogonal decomposition, SIAM J. Sci. Comput. 40 (2018) A3267–A3292.
[45] R. Rubinstein, T.T. Clark, Equilibrium and non-equilibrium turbulence, Theor. Appl. Mech. Lett. 7 (2017) 301–305.